iScience

CellPress
OPEN ACCESS

Article

The Effect of CDK6 Expression on DNA Methylation and DNMT3B Regulation

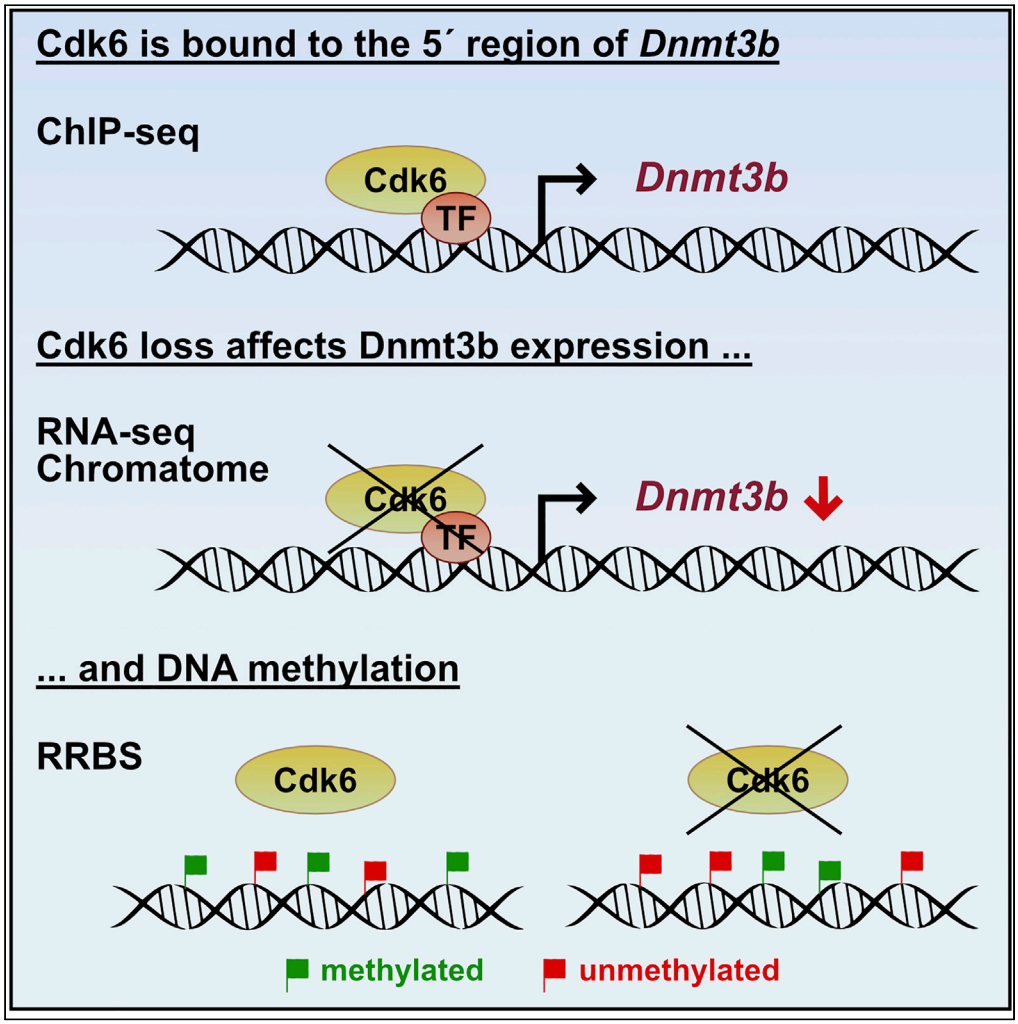

Gerwin Heller, Sofie Nebenfuehr, Florian Bellutti, ..., Lisa Scheiblecker, Veronika Sexl, Karoline Kollmann

veronika.sexl@vetmeduni.ac.at

HIGHLIGHTS

CDK6 and DNMT/TET/HDAC expression correlate in ALL samples

CDK6 transcriptionally regulates DNMT3B in *BCR-ABL*$^+$ cells

DNA methylation patterns change upon CDK6 loss in *BCR-ABL*$^+$ cells

Heller et al., iScience *23*, 101602
October 23, 2020
https://doi.org/10.1016/j.isci.2020.101602

iScience

CellPress
OPEN ACCESS

Article

The Effect of CDK6 Expression on DNA Methylation and DNMT3B Regulation

Gerwin Heller,[1,2,3,4] Sofie Nebenfuehr,[3,4] Florian Bellutti,[3] Huriye Ünal,[3] Markus Zojer,[3] Lisa Scheiblecker,[3] Veronika Sexl,[3,4,5,*] and Karoline Kollmann[3,4]

SUMMARY

CDK6 is frequently overexpressed in various cancer types and functions as a positive regulator of the cell cycle and as a coregulator of gene transcription. We provide evidence that CDK6 is involved in the process of DNA methylation, at least in ALL. We observe a positive correlation of CDK6 and DNMT expression in a large number of ALL samples. ChIP-seq analysis reveals CDK6 binding to genomic regions associated with DNA methyltransferases (DNMTs). ATAC-seq shows a strong reduction in chromatin accessibility for DNMT3B in CDK6-deficient *BCR-ABL*$^{+}$ Cdk6$^{-/-}$ cells, accompanied by lower levels of DNMT3B mRNA and less chromatin-bound DNMT3B, as shown by RNA-seq and chromatome analysis. Motif analysis suggests that ETS family members interact with CDK6 to regulate DNMT3B. Reduced representation bisulfite sequencing analysis uncovers reversible and cell line-specific changes in DNA methylation patterns upon CDK6 loss. The results reveal a function of CDK6 as a regulator of DNA methylation in transformed cells.

INTRODUCTION

The transformation of normal to cancer cells is driven by a multitude of genetic and epigenetic alterations. There is recent evidence that overexpression of the cyclin-dependent kinase 6 (CDK6) is a frequent event in hematological malignancies and solid tumors (Tadesse et al., 2015; Nagel et al., 2008; Tigan et al., 2016). Functional characterization of CDK6 has revealed that it affects a variety of molecular processes (Bellutti et al., 2018; Scheicher et al., 2015; Uras et al., 2017, 2019; Kollmann et al., 2013; Wang et al., 2017). Besides binding D-type cyclins to drive the G1 phase of the cell cycle, it also regulates gene expression (Kollmann et al., 2013; Tigan et al., 2016). Independent of its kinase activity, it interacts with transcription factors to act as a chromatin-bound cofactor that induces or represses the expression of specific genes. We have shown that CDK6 interacts with STAT3 to induce the expression of p16^{INK4a} and with the AP-1 transcription factor c-Jun to induce the expression of VEGF-A (Kollmann et al., 2013). It also cooperates with the NF-κB subunit p65 to induce an inflammatory gene response (Handschick et al., 2014). CDK6 can also repress transcription, as it does in hematopoietic stem cells by interacting with AP-1 to repress EGR1 expression and thereby to induce the exit from quiescence and the growth of leukemic stem cells (Scheicher et al., 2015). Together with NFYA and SP1, CDK6 induces a transcriptional program to block p53 in hematopoietic cells (Bellutti et al., 2018).

Gene transcription is frequently regulated by epigenetic mechanisms, such as DNA methylation, various chemical modifications of histone proteins and chromatin restructuring, which results in gene activation or gene silencing (Sandoval and Esteller, 2012). The main targets of methylation in the mammalian genome are cytosines within CpG dinucleotides. CpG dinucleotides are distributed throughout the genome but are concentrated in regions of about 0.5–2 kb in length, called CpG islands, that are associated with ~60% of human gene promoters (Sandoval and Esteller, 2012). DNA methylation is considered important in the pathogenesis of many solid tumors and hematological malignancies (Heller et al., 2016; Guillamot et al., 2016; Kimura et al., 2019). The CpG islands of many cancer-associated genes are frequently methylated in cancer cells, resulting in the transcriptional silencing of these genes (Sandoval and Esteller, 2012; Heller et al., 2013). Changes in DNA methylation in regions outside CpG islands may be equally important in leukemogenesis, with hypomethylation as relevant as hypermethylation (Guillamot et al., 2016; Figueroa

[1]Department of Medicine I, Division of Oncology, Medical University of Vienna, 1090 Vienna, Austria

[2]Comprehensive Cancer Center, Vienna, Austria

[3]Department for Biomedical Sciences, Institute of Pharmacology and Toxicology, University of Veterinary Medicine Vienna, Veterinaerplatz 1, 1210 Vienna, Austria

[4]These authors contributed equally

[5]Lead Contact

*Correspondence: veronika.sexl@vetmeduni.ac.at

https://doi.org/10.1016/j.isci.2020.101602

et al., 2010; Kimura et al., 2019; Irizarry et al., 2009; Qu et al., 2014). Surprisingly, DNA methylation aberrations in tumor cells of various cancer types are highly heterogeneous (Wenger et al., 2019; Sheffield et al., 2017; Brocks et al., 2014; Li et al., 2016; Landau et al., 2014; Nordlund et al., 2013).

Despite a wealth of evidence, the mechanisms of aberrant methylation in cancer cells remain unclear. There is a preliminary indication that CDK6 may play a part, as inhibition of CDK kinase with palbociclib promotes the degradation of the DNA methyltransferase 1 (DNMT1) (Acevedo et al., 2016). We now confirm that CDK6 is involved in the regulation of DNA methylation, although its function does not depend on its kinase activity. In several independent gene expression microarray datasets from a large number of ALL samples CDK6 is co-expressed with DNMTs, TET1 and histone deacetylases (HDAC). ChIP-seq, ATAC-seq, RNA-seq, and mass spectrometry analysis of chromatin (referred to as chromatome) reveal that DNMT3B is a target for transcriptional regulation by CDK6 in *BCR-ABL*$^{+}$ cells. Reduced representation bisulfite sequencing (RRBS) shows that loss of CDK6 causes changes in DNA methylation patterns in a cell line-specific manner, with both hypomethylation and hypermethylation prominent. Many of the changes in methylation can be reversed by re-expressing CDK6. The findings demonstrate that CDK6 has a function as a regulator of DNA methylation in transformed cells.

RESULTS

CDK6 and DNMT/TET/HDAC Expression Correlate in ALL Samples

Epigenetic changes are frequent in leukemia and epigenetic regulators such as DNMTs and TETs are often mutated in hematopoietic malignancies (Yang et al., 2015, Delhommeau et al., 2009, Cancer Genome Atlas Research Network et al., 2013, Kimura et al., 2019, de Keersmaecker et al., 2013). Coexpression analysis using four independent gene expression microarray data sets from ALL patients showed a positive correlation between levels of CDK6 and of DNMT3A (mean R = 0.46 in 4 data sets; $p < 0.0001$), with an only slightly weaker positive correlation with levels of DNMT3B (mean R = 0.42 in 3 of 4 data sets; $p < 0.0001$) and a weaker correlation with levels of DNMT1 (mean R = 0.34 in 4 data sets; $p < 0.0001$; Figure 1). While CDK6 was positively correlated with TET1 (mean R = 0.49 in 4 data sets; $p < 0.0001$) and negatively with TET2 (mean R = −0.35 in 4 data sets; $p < 0.0001$), there was no correlation with TET3 in ALL patients (Figure 1).

HDACs are also affected in hematopoietic malignancies, although aberrant expression is more common than mutations (Moreno et al., 2010; Zhang et al., 2015). Of the large family of HDACs, we found HDAC1 and HDAC8 to be coexpressed with CDK6 in ALL patients (mean R = 0.55 and 0.42 in 4 data sets; $p < 0.0001$, respectively). The patterns of coexpression between CDK6 and DNMT/TET/HDACs are highly similar in the four gene expression data sets (Figure 1), showing that expression of CDK6 and several factors associated with DNA methylation are positively correlated in ALL. The data suggest that CDK6 might be involved in the changes in DNA methylation during leukemogenesis.

DNMT3B Is Transcriptionally Regulated by CDK6 in *BCR-ABL*$^{+}$ Cells

The transcriptional regulator CDK6 is particularly significant in leukemia, where it is upregulated and contributes to leukemogenesis (Nagel et al., 2008; Tadesse et al., 2015; Tigan et al., 2016). The positive correlation between expression of CDK6 and DNMT3 prompted us to study whether DNMT1, DNMT3A and DNMT3B are transcriptionally regulated by CDK6. Murine (C57Bl/6J) Cdk6^{wt} and Cdk6$^{-/-}$ cell lines obtained from single-cell bone marrow suspension were retrovirally transduced with a pMSCV-BCR-ABLp185-IRES-GFP vector as described (Bellutti et al., 2018). CDK6 ChIP-seq analysis of these cells revealed specific ChIP peaks in the 5′ regions of DNMT1 and DNMT3B (Figures 2A and S1A) and additional CDK6 peaks in the promoter and exonic/intronic regions of DNMT3A (Figure S1B). The chromatin accessibility of the genomic regions harboring the DNMT1 and DNMT3B genes also depended on the presence of CDK6. ATAC-seq analysis in *BCR-ABL*$^{+}$ Cdk6^{wt} and *BCR-ABL*$^{+}$ Cdk6$^{-/-}$ cells showed that the chromatin accessibility in the DNMT3A region was comparable. However, the chromatin accessibility in the DNMT1 and DNMT3B regions was strongly reduced in CDK6-deficient *BCR-ABL*$^{+}$ Cdk6$^{-/-}$ cells (Figures 2A and S1A). The significance of the differences in ATAC-seq were confirmed by RNA-seq analysis, which revealed reduced DNMT3B expression in *BCR-ABL*$^{+}$ Cdk6$^{-/-}$ cells (Figure 2B), while expression of DNMT1 and DNMT3A remained unchanged.

Analysis of the chromatin-bound proteome showed that the changes in transcription are reflected by alterations in protein abundance: less DNMT3B bound to chromatin in *BCR-ABL*$^{+}$ Cdk6$^{-/-}$ cells than in *BCR-ABL*$^{+}$ Cdk6^{wt} cells (Figure 2C). Motif analysis of the genomic region underlying the CDK6

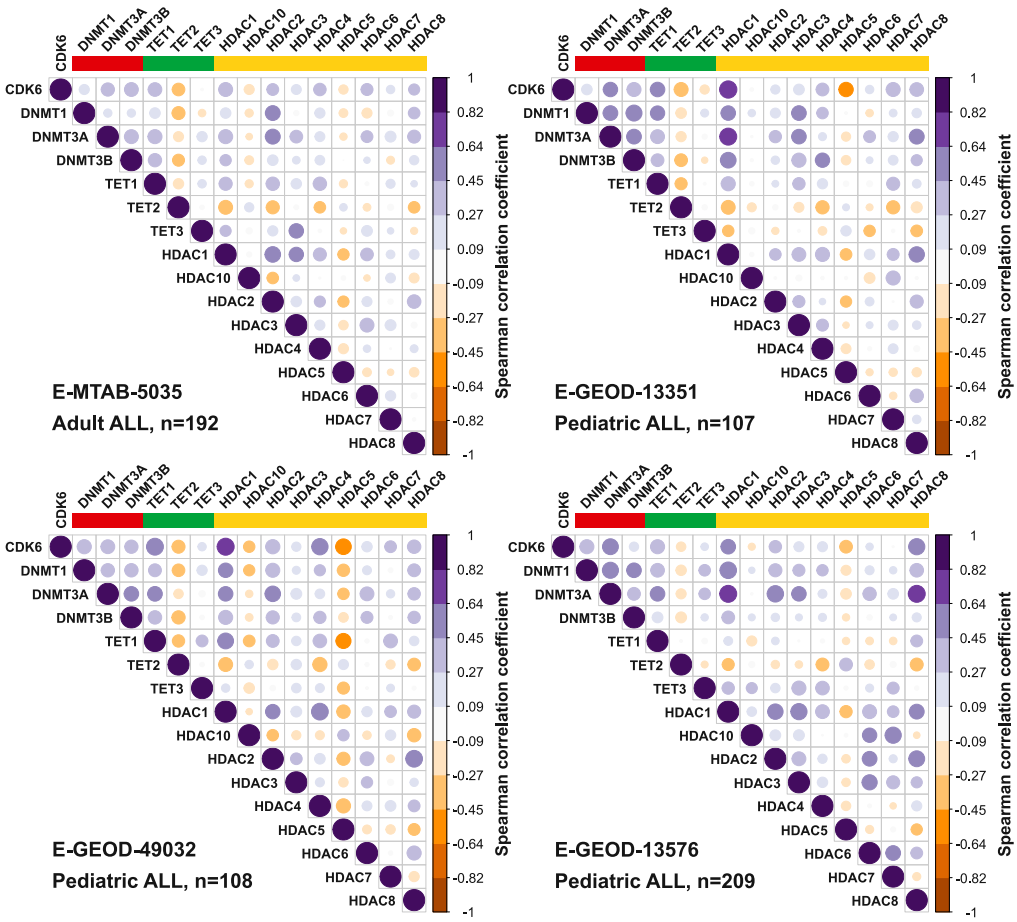

Figure 1. CDK6 and DNMT/TET/HDAC Expression Correlate in ALL Samples

Correlation of CDK6 expression and expression of DNMTs (red), TETs (green) and HDACs (yellow) in 4 independent cohorts of adult or pediatric acute lymphoblastic leukemia (ALL) patients. Spearman correlation coefficients are shown. Blue dots: positive correlation, orange dots: negative correlation.

ChIP-seq/ATAC-seq peak (Figure 2A) identified ETS motifs overlapping with CDK6 binding sites in the 5′ region of *DNMT3B* (Figure 2D). To test if ETS1 binds to this genomic location, we analyzed ETS1 ChIP-seq data from human K562 cells and murine B-cells. We verified that an ETS1 peak overlaps with the CDK6 binding site in the promoter/exon 1 region of DNMT3B in both data sets (Figure 2E). These findings suggest that CDK6 directly regulates DNMT3B, possibly mediated by ETS factors.

DNA Methylation Patterns Change upon Loss of CDK6 in *BCR-ABL*$^+$ Cells

To investigate whether the alterations in DNMT3 expression provoke changes of the methylome, we used a CRISPR-Cas9-based strategy to generate *BCR-ABL*$^+$ cells deficient for CDK6 as confirmed by Western blotting (Figure S2). Our procedure (for details see Transparent Methods) maintains genetic stability and avoids altering p53: CDK6-deficient transformed cells consistently harbor *p53* mutations that may affect the methylome (Tovy et al., 2017). Dnmt3b expression was downregulated upon Cdk6 loss in these cells (Figures 3A and S3). Further, Cdk6 reexpression strongly induced Dnmt3b mRNA expression (Figure 3A). We used 3 individually derived *BCR-ABL*$^+$ cell lines for RRBS to study the methylome. Principal component analysis (PCA) based on CpG site methylation unequivocally separated *BCR-ABL*$^+$ Cdk6$^{-/-}$ cells from *BCR-ABL*$^+$ Cdk6^{wt} cells (Figure 3B). The separation was also evident in the sample correlation plot, which showed weaker correlation between *BCR-ABL*$^+$ Cdk6$^{-/-}$ and *BCR-ABL*$^+$ Cdk6^{wt} cells than within *BCR-ABL*$^+$ Cdk6^{wt} cells (Figure S4).

Unexpectedly, the *BCR-ABL*$^+$ Cdk6$^{-/-}$ samples are not represented in a distinct cluster in the PCA but are separated from one another, indicating that loss of CDK6 is accompanied by different changes in DNA

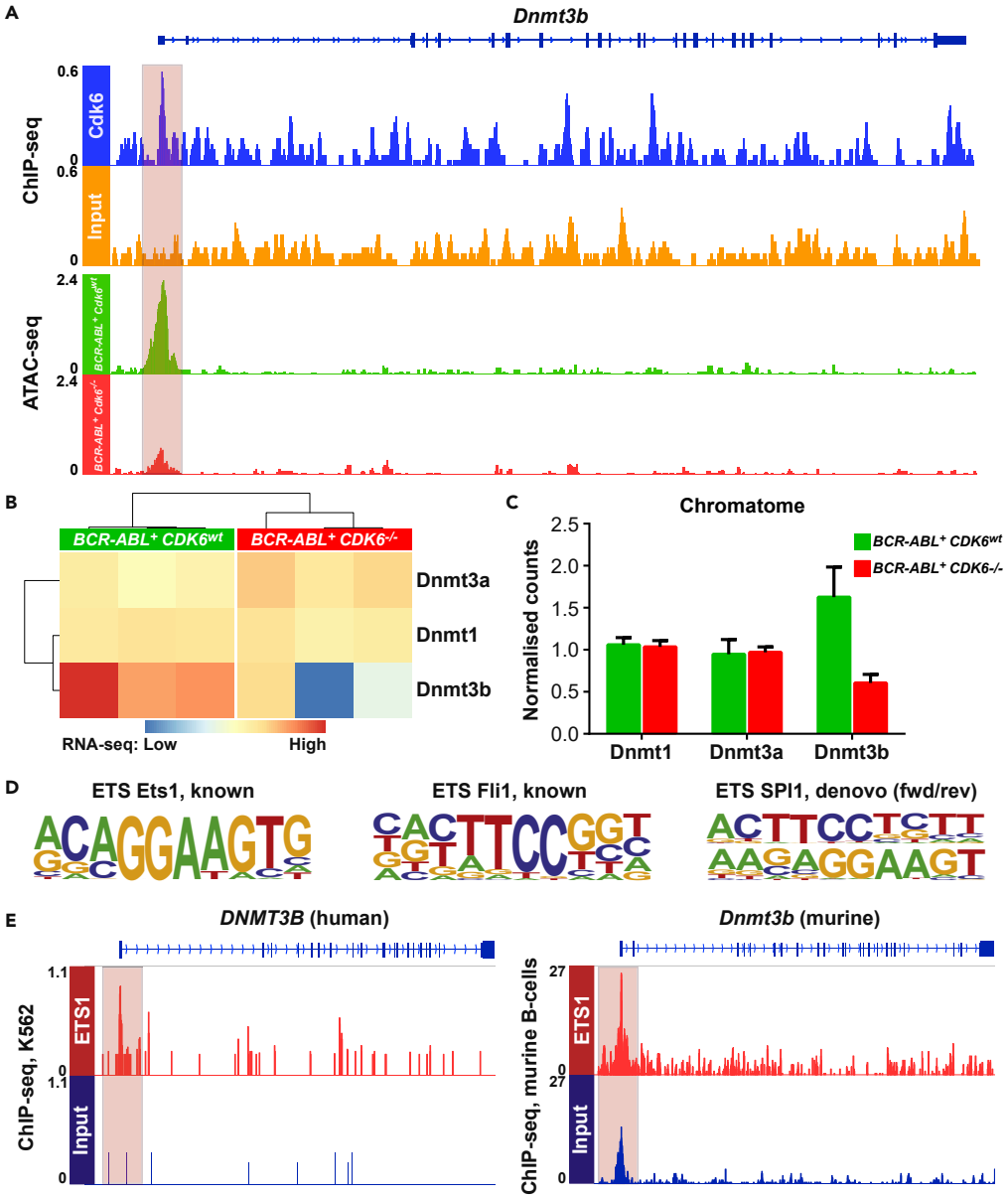

Figure 2. DNMT3B Is Transcriptionally Regulated by CDK6 in *BCR-ABL*$^+$ Cells

(A) Binding of CDK6 to the 5′ region of DNMT3B in *BCR-ABL*$^+$ cells determined by ChIP-seq analysis (upper panel). Chromatin accessibility at the 5′ region of *DNMT3B* in *BCR-ABL*$^+$ Cdk6^{wt} (green) and *BCR-ABL*$^+$ Cdk6$^{-/-}$ (red) cells determined by ATAC-seq analysis. See also Figure S1.

(B) Heatmap showing mRNA expression of DNMT1/3a/3b in *BCR-ABL*$^+$ Cdk6^{wt} (green, N = 3) and *BCR-ABL*$^+$ Cdk6$^{-/-}$ (red, N = 3) cells analyzed by RNA-sequencing.

(C) Chromatin-bound DNMT1/3a/3b in *BCR-ABL*$^+$ Cdk6^{wt} (green) and *BCR-ABL*$^+$ Cdk6$^{-/-}$ (red) cells analyzed by chromatome analysis. Mean values + SD are shown.

(D) ETS motifs found within the ATAC-seq peak at the 5′ UTR of DNMT3B.

(E) Binding of ETS1 to the 5′ region of DNMT3B in human K562 cells (left panel) and in murine spleen cells (right panel) determined by ChIP-seq analysis. See also Figure S1.

methylation in the different cell lines. To investigate the differences in more detail, we examined differential methylation between individual pairs of cell lines. We found 4,707 (2,028 hyper, 2,679 hypo), 4,565 (2,498 hyper, 2,067 hypo) and 5,528 (2,773 hyper, 2,756 hypo) CpG sites with a difference in methylation of at least 40% in each of the three pairwise comparisons (Figure 3C). Only ~1.5% of differentially methylated CpG

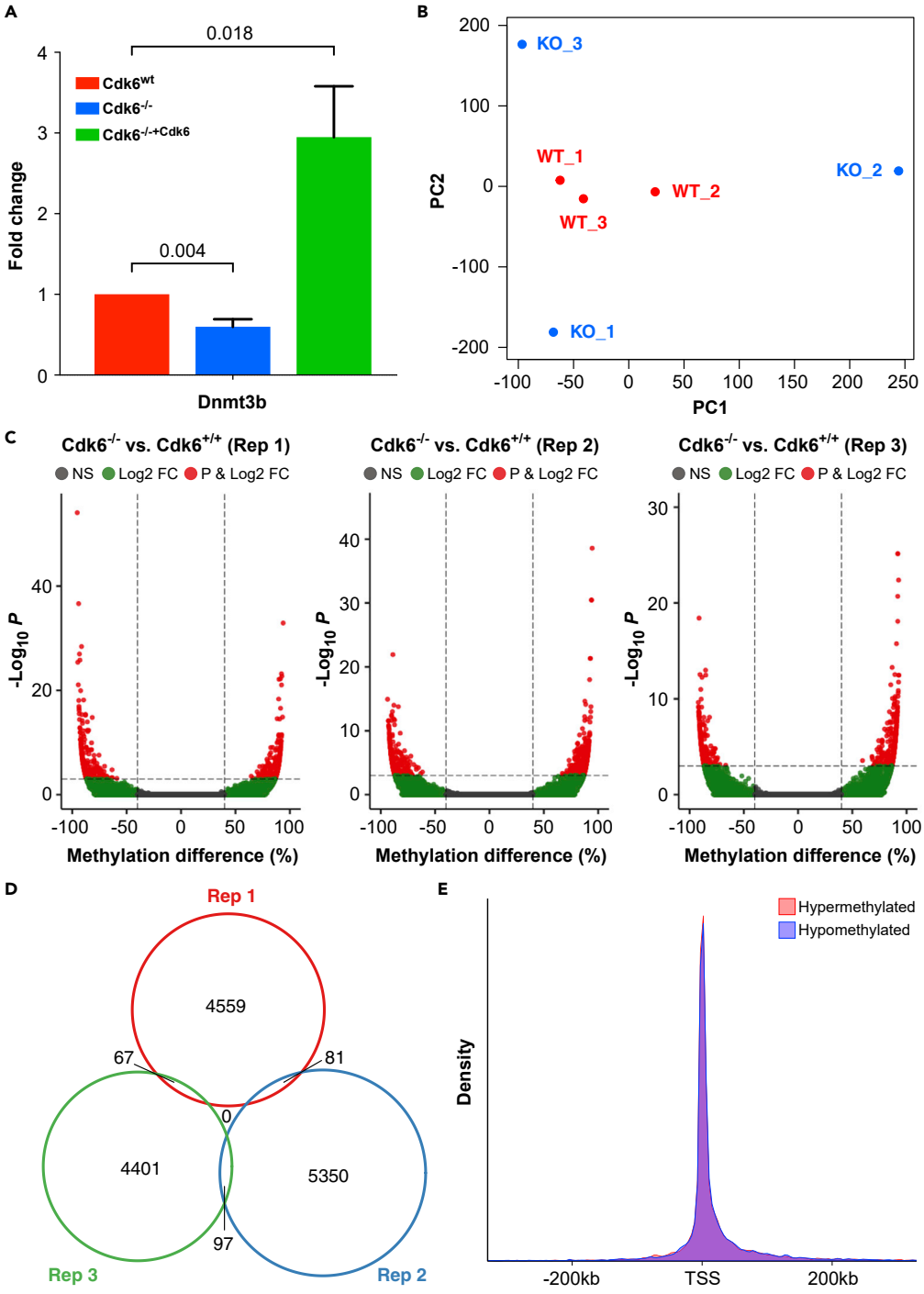

Figure 3. Analysis of the Methylome of *BCR-ABL*$^{+}$ Cdk6^{wt} and *BCR-ABL*$^{+}$ Cdk6$^{-/-}$ Cells By Reduced Representation Bisulfite Sequencing

(A) Quantification of Dnmt3b mRNA expression in *BCR-ABL*$^{+}$ Cdk6^{wt}, *BCR-ABL*$^{+}$ Cdk6$^{-/-}$ and *BCR-ABL*$^{+}$ Cdk6$^{-/-}$+*Cdk6* cells determined by RT-PCR. Mean fold changes +SEM are shown (N = 8), p values were calculated using one-sample t-tests.

(B) Principal component analysis of 3 *BCR-ABL*$^{+}$ Cdk6^{wt} (WT, red) and 3 *BCR-ABL*$^{+}$ Cdk6$^{-/-}$ (KO, blue) cell lines based on CpG methylation. Each dot represents a unique sample. See also Figure S4.

(C) Volcano plots showing hypomethylated and hypermethylated CpG sites in 3 replicates of *BCR-ABL*$^{+}$ Cdk6$^{-/-}$ cell lines compared to *BCR-ABL*$^{+}$ Cdk6^{wt} cells.

Figure 3. *Continued*

(D) Venn diagram illustrating the overlap of differentially methylated CpG sites in the 3 *BCR-ABL*$^{+}$ Cdk6$^{-/-}$ cell lines.
(E) Density plot showing the location of hypermethylated (pink) and hypomethylated (blue) CpG sites relative to transcriptional start sites (TSS). See also Figure S4.

sites were shared in two of the cell lines and no single CpG site showed a consistent difference in methylation in all 3 cell lines (Figure 3D). Annotation of the differentially methylated CpG sites to genomic region revealed that both hyper- and hypomethylated CpG sites are closely associated with transcriptional start sites (TSSs) of genes (Figure 3E). The data confirm that loss of CDK6 has a dramatic effect on DNA methylation in BCR-ABL + cells and suggest that the precise nature of the effect depends on stochastic processes.

In the next step, we asked if DNA methylation changes are also associated with CDK6 expression in patients. Thus, we stratified the TCGA LAML data set into CDK6^{low} (lower quartile, N = 27) and CDK6^{high} (upper quartile, N = 27) samples and tested for correlation between CDK6 and DNMT3B expression as well as for differences in DNA methylation. As for ALL samples (Figure 1), we found a positive correlation between CDK6 and DNMT3B expression in AML samples ($R = 0.47$, $p < 0.005$). Further, CDK6^{high} samples showed a strong increase in methylation (β-difference >0.3) for 1,287 probes (Figure S5). Only 11 probes with decreased methylation (β-difference < -0.3) were found indicating that CDK6 expression is mainly associated with hypermethylation in patient samples.

Expression of CDK6 Reverses Changes in CpG Methylation Caused by Loss of CDK6

It is conceivable that the variable changes in DNA methylation are a result of different levels of CDK6. We tested this possibility by re-expressing CDK6 using retroviral transduction with a construct encoding HA-CDK6 (Figure S2) and RRBS analysis and compared methylation in the reconstituted *BCR-ABL*$^{+}$ Cdk6$^{-/-}$+*Cdk6* cells and the maternal cells (*BCR-ABL*$^{+}$ Cdk6^{wt} and *BCR-ABL*$^{+}$ Cdk6$^{-/-}$). Re-expression of CDK6 did not result in the formation of a separate methylation cluster in the hierarchical cluster analysis but showed that *BCR-ABL*$^{+}$ Cdk6$^{-/-}$+*Cdk6* cells clustered with *BCR-ABL*$^{+}$ Cdk6$^{-/-}$ cells from the same background (Figure 4A). Thus, re-expression of CDK6 does not induce global changes of the methylome but regulates a distinct set of genes in each cell line. We then analyzed whether the methylation changes caused by loss of CDK6 are reverted by re-expression of CDK6. Hypomethylation of 79% (range: 70%–85%) of CpG sites was found to be reversible (>1.5-fold increase in methylation) in the three cell lines, while methylation of 34% of the hypermethylated CpG sites (mean: 34%; range: 26%–48%) was reverted when CDK6 is re-expressed (Figure 4B). The reversal of methylation patterns was independent of the location of CpG sites and was found consistently in CGIs, CGI shores, CGI shelves, inter CGI regions, promoters, introns, exons, and intergenic regions (Figure S6). The effect of re-expression of CDK6 on the methylation of 5,000 randomly selected CpG sites was weak (mean methylation changes: 6.6%; repeated 10 times), confirming that the changes in methylation mediated by CDK6 re-expression are specific (Figure S7).

As the re-expression of CDK6 produces varying amounts of the protein in the individual cells, the consistent nature of the changes in methylation caused by re-expression of CDK6 shows that the changes are independent of the level of CDK6. In other words, expression of CDK6 is associated with specific changes in CpG methylation, with the precise effects different for each individual clone. Re-expression of CDK6 largely reverts the hypomethylation mediated by loss of CDK6, although the hypermethylation in *BCR-ABL*$^{+}$ Cdk6$^{-/-}$ cells is only partially revertable, strengthening the dominating hypermethylation seen in CDK6^{high} patient samples (Figure S5).

CDK6-Dependent Differential Methylation Is Associated with Altered Gene Expression in *BCR-ABL*$^{+}$ Cells

Loss of CDK6 is thus associated with changes in DNA methylation. As not all changes in DNA methylation result in differences in gene regulation, we performed RNA-seq analysis to examine the consequences of loss of CDK6 on gene expression. PCA based on all gene expression data revealed that *BCR-ABL*$^{+}$ Cdk6$^{-/-}$ cells and *BCR-ABL*$^{+}$ Cdk6^{wt} cells cluster separately with lower heterogeneity than the RRBS clustering (Figure S8). The overlay of CDK6-dependent methylation and transcriptional regulation uncovered an inverse pattern of decreased methylation/increased gene expression or increased methylation/decreased gene expression for 12 (2 up, 10 down), 29 (16 up, 13 down) and 14 (8 up, 6 down) genes in the three cell lines (Figure 5A). *In silico* functional characterization of these genes identified them as involved in cell differentiation (e.g. *Runx2*, *Shox2*, *Shb*), cell proliferation (e.g. *Fzd3*, *Satb1*, *TBX2*), immune systems (e.g. *Gfi1*,

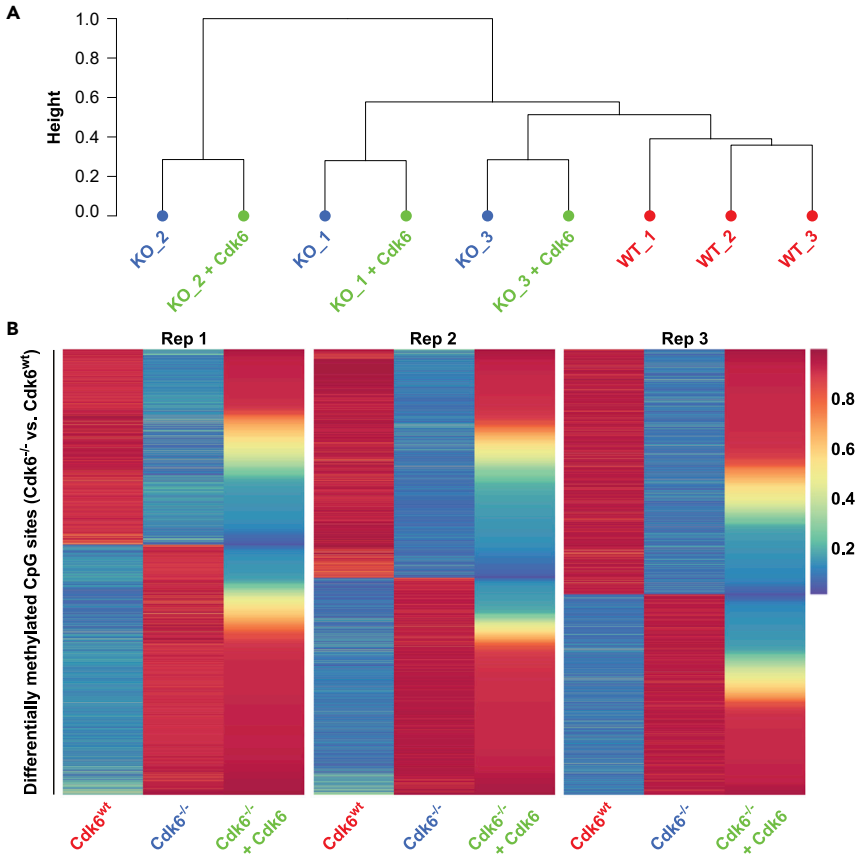

Figure 4. Reversal of CDK6 Loss Mediated CpG Site Methylation Changes by CDK6 Re-expression

(A) Dendrogram of hierarchical clustering of *BCR-ABL*$^{+}$ Cdk6^{wt} (WT, red), *BCR-ABL*$^{+}$ Cdk6$^{-/-}$ (KO, blue) and *BCR-ABL*$^{+}$ Cdk6$^{-/-}$+*Cdk6* (KO + CDK6, green) cells based on CpG site methylation.

(B) Heatmaps showing methylation values of differentially methylated CpG sites in 3 replicates (Rep 1–3) of *BCR-ABL*$^{+}$ Cdk6^{wt}, *BCR-ABL*$^{+}$ Cdk6$^{-/-}$ and *BCR-ABL*$^{+}$ Cdk6$^{-/-}$+*Cdk6* cell lines. Values are depicted as percentage of methylation and range from 0% (dark blue) to 100% (dark red). See also Figures S6 and S7.

Nfkbiz), MAPK signaling (e.g. *Dusp4*, *Mlkl*), Wnt signaling (e.g. *Fzd3*, *Fzd6*) or cell growth regulation (e.g. *Lhx2*, *Bcl6*) (Figure 5B). This shows that various genes involved in cancer-related pathways are transcriptionally deregulated by CDK6-mediated changes in DNA methylation.

DISCUSSION

We show for the first time that CDK6 directly affects DNA methylation in a cell-specific manner. Global demethylation and de novo methylation of selected CpG islands are key events in the pathogenesis of malignant diseases (Michalak et al., 2019; Zhou et al., 2018). During the past decade, tremendous effort has been spent to identify the mechanisms of these epigenetic alterations in cancer cells and a variety of molecular changes have been associated with deregulated DNA methylation. Large-scale studies have shown that certain genes encoding enzymes involved in DNA methylation are affected by somatic mutations in certain types of cancer (Cancer Genome Atlas Research Network et al., 2013; Walter et al., 2011; Ley et al., 2010). Mutations of DNA methyltransferases (DNMTs), especially of *DNMT3A*, *TET2*, *IDH1*, and *IDH2*, have been found in AML and other hematopoietic malignancies (Yang et al., 2015; Spencer et al., 2017; Delhommeau et al., 2009; Paschka et al., 2010, Cancer Genome Atlas Research Network et al., 2013) and deregulated expression of DNMTs has been found in multiple tumor types, resulting in aberrant DNA methylation (Esteller, 2008; Peng et al., 2006; Saito et al., 2003).

We show that expression of DNMT3 and other epigenetic modifiers correlates with CDK6 expression in ALL patients. To investigate the mechanism we used a multi-omics approach in *BCR-ABL*$^{+}$ cells. ChIP-seq

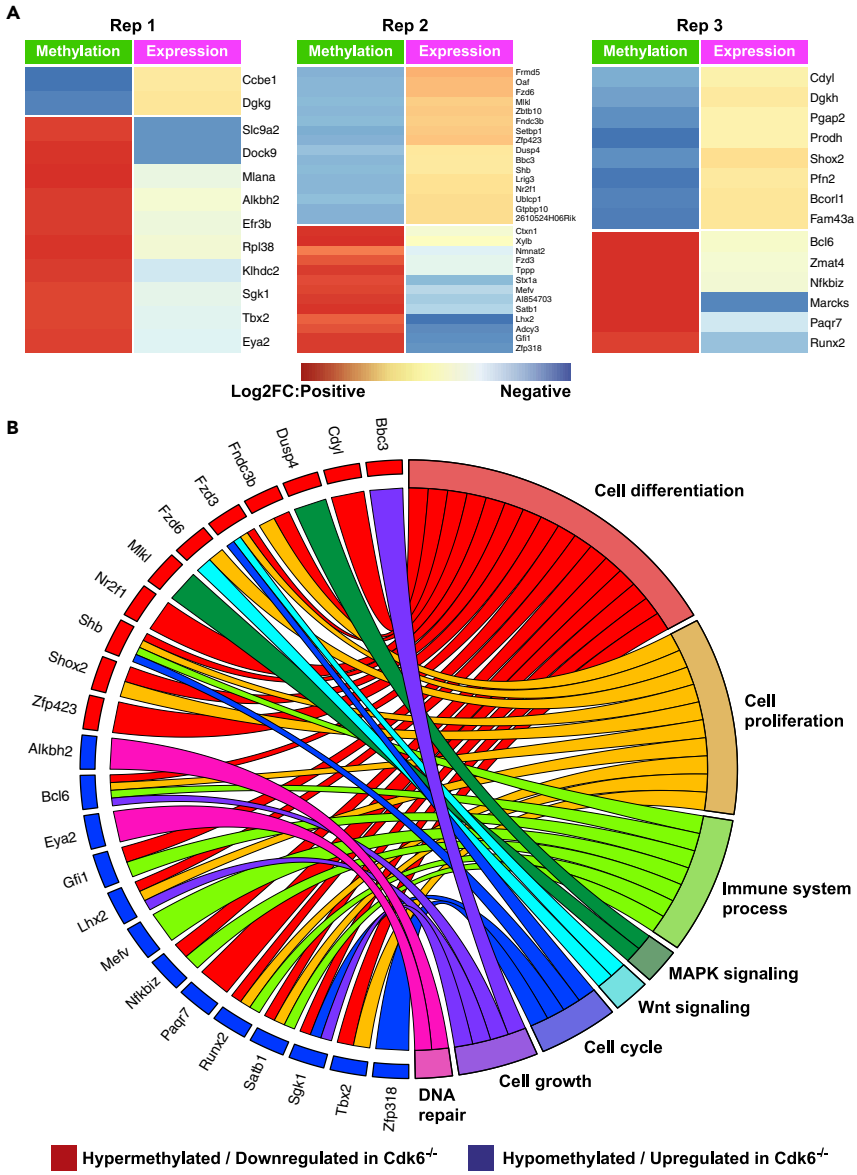

Figure 5. Correlation of Differential Methylation and Gene Expression in *BCR-ABL*$^{+}$ Cdk6$^{-/-}$ Cells Compared to *BCR-ABL*$^{+}$ Cdk6^{wt} Cells

(A) Heatmaps showing fold changes in DNA methylation (green panels) and gene expression (violet panels) determined by RNA-sequencing. Fold changes range from red (positive) to blue (negative). The 3 cell lines are presented separately.
(B) Association of hypermethylated/downregulated genes (red rectangles) and hypomethylated/upregulated genes (blue rectangles) with certain cancer-related molecular pathways. See also Figure S8.

analysis showed that CDK6 is located at multiple sites within the 5′ regions and/or intragenic regions of DNMTs. In the case of DNMT3B, ATAC-seq and RNA-seq analysis associated CDK6 binding with open chromatin and transcriptional regulation. The regulation of DNMT3B mediated by CDK6 is reflected on the protein level and chromatome analysis showed reduced levels of DNMT3B protein in CDK6-deficient cells. Of note, we observed a correlation between CDK6 and TET1 expression in the ALL datasets. However, because TET1 expression was not detected in our experimental system, this correlation was not further investigated.

While the frequency of *DNMT3B* mutations in cancer cells is generally low, deregulated expression of this gene is of potential clinical relevance in multiple cancer types (Hayette et al., 2012; Lamba et al., 2018;

Niederwieser et al., 2015; Poole et al., 2017; Amara et al., 2010; Ibrahim et al., 2011). Overexpression of DNMT3B has been correlated with shorter event-free survival (EFS) and a trend toward poorer overall survival (OS) in a large panel of *de novo* AML patients (Hayette et al., 2012). Increased expression of DNMT3B has also been associated with poor clinical outcome, worse minimal residual disease, high rate of relapse or resistant disease and worse EFS in pediatric AML patients (Lamba et al., 2018) and older adults with primary, cytogenetically normal AML, and high levels of DNMT3B had fewer complete remissions, inferior disease-free survival, and shorter OS (Niederwieser et al., 2015). Prognostically relevant overexpression of DNMT3B is not confined to AML patients. It has also been described for patients with diffuse large B-cell lymphomas and DNMT3B overexpression was detected in clinical specimens from T-ALL and Burkitt's lymphoma patients (Poole et al., 2017; Amara et al., 2010). We observed heterogeneous expression of DNMT3A/B, with levels positively correlating with levels of CDK6 in adult or pediatric ALL samples (Figure 1). This supports the idea that the regulatory effect of CDK6 is not confined to our *in vitro* experiments but is also relevant *in vivo*.

CDK6 does not have a DNA-binding domain, so can only bind to DNA in conjunction with transcription factors. Such cooperations have been observed between CDK6 and STAT3, c-Jun, p65, AP-1, NFYA, and SP1 and result in the transcriptional regulation of specific target genes (Kollmann et al., 2013; Handschick et al., 2014; Scheicher et al., 2015; Bellutti et al., 2018). To determine which transcription factor interacts with CDK6 on the 5′ region of DNMT3B, we performed motif analysis of the region underlying the ChIP-seq/ATAC-seq peak as shown in Figure 2A. ETS motifs are the predominant binding sites and ETS1 ChIP-seq analysis identified ETS1 peaks in the DNMT3B 5′ region in human *BCR-ABL*$^{+}$ K562 cells as well as murine B-cells. These data suggest that DNMT3B may be regulated by the binding of CDK6/ETS family to its promoter region. This idea will be addressed in further studies.

To determine whether CDK6 affects the methylome we used the next-generation sequencing approach RRBS to perform extensive methylation analysis in *BCR-ABL*$^{+}$ cells either expressing or lacking CDK6. We found both hypermethylation and hypomethylation. Although the numbers of differentially methylated CpG sites in different cell lines were comparable, we failed to detect a common pattern of differential methylation. It is attractive to speculate that this observation reflects the heterogeneity in tumor DNA methylation that has been described for various types of human cancer (Wenger et al., 2019; Sheffield et al., 2017; Brocks et al., 2014; Li et al., 2016; Landau et al., 2014; Nordlund et al., 2013). Our result is consistent with the report that aberrant DNA methylation is a signature for the heterogeneity of ALL patients of similar cytogenetic backgrounds (Nordlund et al., 2013). Importantly, many of the methylation changes mediated by CDK6 can be reverted by re-expressing CDK6. This indicates that CDK6 is directly involved in the process of DNA methylation rather than inducing secondary methylation changes. Our finding is consistent with indications that CDK6 is involved in epigenetic programming, such as the observation that DNMT1 is degraded by inhibition of CDK6 with the CDK4/6 inhibitor palbociclib (Acevedo et al., 2016) and that the CDK4/6 inhibitor abemaciclib causes cell cycle inhibition and changes DNA demethylation and immunogenicity (Dowless et al., 2018). However, we provide the first evidence of a direct effect of CDK6 on methylation.

The molecular consequences of the changes in DNA methylation mediated by CDK6 are unclear. It is possible that CDK6 does more than regulate gene transcription, conceivably also having effects on transcription factor binding and chromatin organization. DNA methylation can either mask consensus DNA-binding sites or create new binding sites for transcription factors and nuclear complexes (Bartke et al., 2010; Spruijt et al., 2013). The transcription factor CTCF, which is involved in large-scale chromatin organization, is known to be methylation-sensitive (Bell and Felsenfeld, 2000; Hashimoto et al., 2017; Ghirlando and Felsenfeld, 2016). DNA methylation prevents CTCF binding, thus, CDK6-mediated changes in DNA methylation may be associated with establishing and/or maintaining higher-order topological structures in the genome.

In summary, we show that loss of CDK6 contributes to DNA hypomethylation and hypermethylation. Importantly, the effect of CDK6 on DNA methylation is generally reversible, a point that should be considered when targeting CDK6 in anticancer therapy. We also identify DNMT3B as a transcriptional target of CDK6. This function of CDK6 was unknown so far but the extent to which CDK6-dependent changes in DNA methylation contribute to tumorigenesis and the maintenance of a malignant phenotype remains to be determined.

Limitations of the Study

In the present study, we demonstrated that CDK6 affects DNA methylation by transcriptional regulation of DNMT3B. However, because CDK6 does not have a DNA-binding domain, it can only bind to DNA in association with transcription factors. Our data suggest that ETS1 is one of these factors but the interaction between CDK6 and ETS1 remains to be investigated in more detail.

Resource Availability

Lead Contact

Further information and requests for resources and reagents should be directed to and will be fulfilled by the Lead Contact, Veronika Sexl (Veronika.Sexl@vetmeduni.ac.at).

Materials Availability

This study did not generate new unique reagents.

All reagents generated in this study are available from the Lead Contact with a completed Materials Transfer Agreement.

Data Availability and Code Availability

The accession numbers for the data sets reported in this paper are: GEO: GSE145220, GEO: GSE156966, GEO: GSE145220, GEO: GSE113752.

METHODS

All methods can be found in the accompanying Transparent Methods supplemental file.

SUPPLEMENTAL INFORMATION

Supplemental Information can be found online at https://doi.org/10.1016/j.isci.2020.101602.

ACKNOWLEDGMENTS

The authors thank Graham Tebb for scientific discussions and editing of the manuscript. This work was supported by the European Research Council (ERC) under the European Union's Horizon 2020 research and innovation program grant agreement No 694354 to VS and by the Austrian Science Fund, project P-31773 to KK.

AUTHOR CONTRIBUTIONS

GH performed bioinformatic data analysis, data visualization, and wrote the manuscript; SN, FB, HÜ, LS, and KK performed wet lab experiments; MZ performed bioinformatic data analysis; VS and KK supervised the project team and wrote the manuscript; all authors carefully proof-read the manuscript.

DECLARATION OF INTERESTS

The authors declare no competing interests.

Received: May 6, 2020
Revised: August 31, 2020
Accepted: September 21, 2020
Published: October 23, 2020

REFERENCES

Acevedo, M., Vernier, M., Mignacca, L., Lessard, F., Huot, G., Moiseeva, O., Bourdeau, V., and Ferbeyre, G. (2016). A CDK4/6-dependent epigenetic mechanism protects cancer cells from PML-induced senescence. Cancer Res. *76*, 3252–3264.

Amara, K., Ziadi, S., Hachana, M., Soltani, N., Korbi, S., and Trimeche, M. (2010). DNA methyltransferase DNMT3b protein overexpression as a prognostic factor in patients with diffuse large B-cell lymphomas. Cancer Sci. *101*, 1722–1730.

Bartke, T., Vermeulen, M., Xhemalce, B., Robson, S.C., Mann, M., and Kouzarides, T. (2010). Nucleosome-interacting proteins regulated by DNA and histone methylation. Cell *143*, 470–484.

Bell, A.C., and Felsenfeld, G. (2000). Methylation of a CTCF-dependent boundary controls imprinted expression of the Igf2 gene. Nature *405*, 482–485.

Bellutti, F., Tigan, A.S., Nebenfuehr, S., Dolezal, M., Zojer, M., Grausenburger, R., Hartenberger, S., Kollmann, S., Doma, E., Prchal-Murphy, M., et al. (2018). CDK6 antagonizes p53-induced

responses during tumorigenesis. Cancer Discov. *8*, 884–897.

Brocks, D., Assenov, Y., Minner, S., Bogatyrova, O., Simon, R., Koop, C., Oakes, C., Zucknick, M., Lipka, D.B., Weischenfeldt, J., et al. (2014). Intratumor DNA methylation heterogeneity reflects clonal evolution in aggressive prostate cancer. Cell Rep. *8*, 798–806.

Cancer Genome Atlas Research Network, Ley, T.J., Miller, C., Ding, L., Raphael, B.J., Mungall, A.J., Robertson, A., Hoadley, K., Triche, T.J., Jr., Laird, P.W., et al. (2013). Genomic and epigenomic landscapes of adult de novo acute myeloid leukemia. N. Engl. J. Med. *368*, 2059–2074.

de Keersmaecker, K., Atak, Z.K., Li, N., Vicente, C., Patchett, S., Girardi, T., Gianfelici, V., Geerdens, E., Clappier, E., Porcu, M., et al. (2013). Exome sequencing identifies mutation in CNOT3 and ribosomal genes RPL5 and RPL10 in T-cell acute lymphoblastic leukemia. Nat. Genet. *45*, 186–190.

Delhommeau, F., Dupont, S., Della Valle, V., James, C., Trannoy, S., Masse, A., Kosmider, O., Le Couedic, J.P., Robert, F., Alberdi, A., et al. (2009). Mutation in TET2 in myeloid cancers. N. Engl. J. Med. *360*, 2289–2301.

Dowless, M., Lowery, C.D., Shackleford, T., Renschler, M., Stephens, J., Flack, R., Blosser, W., Gupta, S., Stewart, J., Webster, Y., et al. (2018). Abemaciclib is active in preclinical models of ewing sarcoma via multipronged regulation of cell cycle, DNA methylation, and interferon pathway signaling. Clin. Cancer Res. *24*, 6028–6039.

Esteller, M. (2008). Epigenetics in cancer. N. Engl. J. Med. *358*, 1148–1159.

Figueroa, M.E., Lugthart, S., Li, Y., Erpelinck-Verschueren, C., Deng, X., Christos, P.J., Schifano, E., Booth, J., Van Putten, W., Skrabanek, L., et al. (2010). DNA methylation signatures identify biologically distinct subtypes in acute myeloid leukemia. Cancer Cell *17*, 13–27.

Ghirlando, R., and Felsenfeld, G. (2016). CTCF: making the right connections. Genes Dev. *30*, 881–891.

Guillamot, M., Cimmino, L., and Aifantis, I. (2016). The impact of DNA methylation in hematopoietic malignancies. Trends Cancer *2*, 70–83.

Handschick, K., Beuerlein, K., Jurida, L., Bartkuhn, M., Muller, H., Soelch, J., Weber, A., Dittrich-Breiholz, O., Schneider, H., Scharfe, M., et al. (2014). Cyclin-dependent kinase 6 is a chromatin-bound cofactor for NF-kappaB-dependent gene expression. Mol. Cell *53*, 193–208.

Hashimoto, H., Wang, D., Horton, J.R., Zhang, X., Corces, V.G., and Cheng, X. (2017). Structural basis for the versatile and methylation-dependent binding of CTCF to DNA. Mol. Cell *66*, 711–720 e3.

Hayette, S., Thomas, X., Jallades, L., Chabane, K., Charlot, C., Tigaud, I., Gazzo, S., Morisset, S., Cornillet-Lefebvre, P., Plesa, A., et al. (2012). High DNA methyltransferase DNMT3B levels: a poor prognostic marker in acute myeloid leukemia. PLoS One *7*, e51527.

Heller, G., Babinsky, V.N., Ziegler, B., Weinzierl, M., Noll, C., Altenberger, C., Mullauer, L., Dekan, G., Grin, Y., Lang, G., et al. (2013). Genome-wide CpG island methylation analyses in non-small cell lung cancer patients. Carcinogenesis *34*, 513–521.

Heller, G., Topakian, T., Altenberger, C., Cerny-Reiterer, S., Herndlhofer, S., Ziegler, B., Datlinger, P., Byrgazov, K., Bock, C., Mannhalter, C., et al. (2016). Next-generation sequencing identifies major DNA methylation changes during progression of Ph+ chronic myeloid leukemia. Leukemia *30*, 1861–1868.

Ibrahim, A.E., Arends, M.J., Silva, A.L., Wyllie, A.H., Greger, L., Ito, Y., Vowler, S.L., Huang, T.H., Tavare, S., Murrell, A., and Brenton, J.D. (2011). Sequential DNA methylation changes are associated with DNMT3B overexpression in colorectal neoplastic progression. Gut *60*, 499–508.

Irizarry, R.A., Ladd-Acosta, C., Wen, B., Wu, Z., Montano, C., Onyango, P., Cui, H., Gabo, K., Rongione, M., Webster, M., et al. (2009). The human colon cancer methylome shows similar hypo- and hypermethylation at conserved tissue-specific CpG island shores. Nat. Genet. *41*, 178–186.

Kimura, S., Seki, M., Kawai, T., Goto, H., Yoshida, K., Isobe, T., Sekiguchi, M., Watanabe, K., Kubota, Y., Nannya, Y., et al. (2019). DNA methylation-based classification reveals difference between pediatric T-cell acute lymphoblastic leukemia and normal thymocytes. Leukemia *34*, 1163–1168.

Kollmann, K., Heller, G., Schneckenleithner, C., Warsch, W., Scheicher, R., Ott, R.G., Schafer, M., Fajmann, S., Schlederer, M., Schiefer, A.I., et al. (2013). A kinase-independent function of CDK6 links the cell cycle to tumor angiogenesis. Cancer Cell *24*, 167–181.

Lamba, J.K., Cao, X., Raimondi, S.C., Rafiee, R., Downing, J.R., Lei, S., Gruber, T., Ribeiro, R.C., Rubnitz, J.E., and Pounds, S.B. (2018). Integrated epigenetic and genetic analysis identifies markers of prognostic significance in pediatric acute myeloid leukemia. Oncotarget *9*, 26711–26723.

Landau, D.A., Clement, K., Ziller, M.J., Boyle, P., Fan, J., Gu, H., Stevenson, K., Sougnez, C., Wang, L., Li, S., et al. (2014). Locally disordered methylation forms the basis of intratumor methylome variation in chronic lymphocytic leukemia. Cancer Cell *26*, 813–825.

Ley, T.J., Ding, L., Walter, M.J., Mclellan, M.D., Lamprecht, T., Larson, D.E., Kandoth, C., Payton, J.E., Baty, J., Welch, J., et al. (2010). DNMT3A mutations in acute myeloid leukemia. N. Engl. J. Med. *363*, 2424–2433.

Li, S., Garrett-Bakelman, F.E., Chung, S.S., Sanders, M.A., Hricik, T., Rapaport, F., Patel, J., Dillon, R., Vijay, P., Brown, A.L., et al. (2016). Distinct evolution and dynamics of epigenetic and genetic heterogeneity in acute myeloid leukemia. Nat. Med. *22*, 792–799.

Michalak, E.M., Burr, M.L., Bannister, A.J., and Dawson, M.A. (2019). The roles of DNA, RNA and histone methylation in ageing and cancer. Nat. Rev. Mol. Cell Biol. *20*, 573–589.

Moreno, D.A., Scrideli, C.A., Cortez, M.A., De Paula Queiroz, R., Valera, E.T., Da Silva Silveira, V., Yunes, J.A., Brandalise, S.R., and Tone, L.G. (2010). Differential expression of HDAC3, HDAC7 and HDAC9 is associated with prognosis and survival in childhood acute lymphoblastic leukaemia. Br. J. Haematol. *150*, 665–673.

Nagel, S., Leich, E., Quentmeier, H., Meyer, C., Kaufmann, M., Drexler, H.G., Zettl, A., Rosenwald, A., and Macleod, R.A. (2008). Amplification at 7q22 targets cyclin-dependent kinase 6 in T-cell lymphoma. Leukemia *22*, 387–392.

Niederwieser, C., Kohlschmidt, J., Volinia, S., Whitman, S.P., Metzeler, K.H., Eisfeld, A.K., Maharry, K., Yan, P., Frankhouser, D., Becker, H., et al. (2015). Prognostic and biologic significance of DNMT3B expression in older patients with cytogenetically normal primary acute myeloid leukemia. Leukemia *29*, 567–575.

Nordlund, J., Backlin, C.L., Wahlberg, P., Busche, S., Berglund, E.C., Eloranta, M.L., Flaegstad, T., Forestier, E., Frost, B.M., Harila-Saari, A., et al. (2013). Genome-wide signatures of differential DNA methylation in pediatric acute lymphoblastic leukemia. Genome Biol. *14*, r105.

Paschka, P., Schlenk, R.F., Gaidzik, V.I., Habdank, M., Kronke, J., Bullinger, L., Spath, D., Kayser, S., Zucknick, M., Gotze, K., et al. (2010). IDH1 and IDH2 mutations are frequent genetic alterations in acute myeloid leukemia and confer adverse prognosis in cytogenetically normal acute myeloid leukemia with NPM1 mutation without FLT3 internal tandem duplication. J. Clin. Oncol. *28*, 3636–3643.

Peng, D.F., Kanai, Y., Sawada, M., Ushijima, S., Hiraoka, N., Kitazawa, S., and Hirohashi, S. (2006). DNA methylation of multiple tumor-related genes in association with overexpression of DNA methyltransferase 1 (DNMT1) during multistage carcinogenesis of the pancreas. Carcinogenesis *27*, 1160–1168.

Poole, C.J., Zheng, W., Lodh, A., Yevtodiyenko, A., Liefwalker, D., Li, H., Felsher, D.W., and Van Riggelen, J. (2017). DNMT3B overexpression contributes to aberrant DNA methylation and MYC-driven tumor maintenance in T-ALL and Burkitt's lymphoma. Oncotarget *8*, 76898–76920.

Qu, Y., Lennartsson, A., Gaidzik, V.I., Deneberg, S., Karimi, M., Bengtzen, S., Hoglund, M., Bullinger, L., Dohner, K., and Lehmann, S. (2014). Differential methylation in CN-AML preferentially targets non-CGI regions and is dictated by DNMT3A mutational status and associated with predominant hypomethylation of HOX genes. Epigenetics *9*, 1108–1119.

Saito, Y., Kanai, Y., Nakagawa, T., Sakamoto, M., Saito, H., Ishii, H., and Hirohashi, S. (2003). Increased protein expression of DNA methyltransferase (DNMT) 1 is significantly correlated with the malignant potential and poor prognosis of human hepatocellular carcinomas. Int. J. Cancer *105*, 527–532.

Sandoval, J., and Esteller, M. (2012). Cancer epigenomics: beyond genomics. Curr. Opin. Genet. Dev. *22*, 50–55.

Scheicher, R., Hoelbl-Kovacic, A., Bellutti, F., Tigan, A.S., Prchal-Murphy, M., Heller, G., Schneckenleithner, C., Salazar-Roa, M., Zochbauer-Muller, S., Zuber, J., et al. (2015).

CDK6 as a key regulator of hematopoietic and leukemic stem cell activation. Blood *125*, 90–101.

Sheffield, N.C., Pierron, G., Klughammer, J., Datlinger, P., Schonegger, A., Schuster, M., Hadler, J., Surdez, D., Guillemot, D., Lapouble, E., et al. (2017). DNA methylation heterogeneity defines a disease spectrum in Ewing sarcoma. Nat. Med. *23*, 386–395.

Spencer, D.H., Russler-Germain, D.A., Ketkar, S., Helton, N.M., Lamprecht, T.L., Fulton, R.S., Fronick, C.C., O'laughlin, M., Heath, S.E., Shinawi, M., et al. (2017). CpG island hypermethylation mediated by DNMT3A is a consequence of AML progression. Cell *168*, 801–816 e13.

Spruijt, C.G., Gnerlich, F., Smits, A.H., Pfaffeneder, T., Jansen, P.W., Bauer, C., Munzel, M., Wagner, M., Muller, M., Khan, F., et al. (2013). Dynamic readers for 5-(hydroxy)methylcytosine and its oxidized derivatives. Cell *152*, 1146–1159.

Tadesse, S., Yu, M., Kumarasiri, M., Le, B.T., and Wang, S. (2015). Targeting CDK6 in cancer: state of the art and new insights. Cell Cycle *14*, 3220–3230.

Tigan, A.S., Bellutti, F., Kollmann, K., Tebb, G., and Sexl, V. (2016). CDK6-a review of the past and a glimpse into the future: from cell-cycle control to transcriptional regulation. Oncogene *35*, 3083–3091.

Tovy, A., Spiro, A., Mccarthy, R., Shipony, Z., Aylon, Y., Allton, K., Ainbinder, E., Furth, N., Tanay, A., Barton, M., and Oren, M. (2017). p53 is essential for DNA methylation homeostasis in naive embryonic stem cells, and its loss promotes clonal heterogeneity. Genes Dev. *31*, 959–972.

Uras, I.Z., Maurer, B., Nivarthi, H., Jodl, P., Kollmann, K., Prchal-Murphy, M., Milosevic Feenstra, J.D., Zojer, M., Lagger, S., Grausenburger, R., et al. (2019). CDK6 coordinates JAK2 (V617F) mutant MPN via NF-kappaB and apoptotic networks. Blood *133*, 1677–1690.

Uras, I.Z., Scheicher, R.M., Kollmann, K., Glosmann, M., Prchal-Murphy, M., Tigan, A.S., Fux, D.A., Altamura, S., Neves, J., Muckenthaler, M.U., et al. (2017). Cdk6 contributes to cytoskeletal stability in erythroid cells. Haematologica *102*, 995–1005.

Walter, M.J., Ding, L., Shen, D., Shao, J., Grillot, M., Mclellan, M., Fulton, R., Schmidt, H., Kalicki-Veizer, J., O'laughlin, M., et al. (2011). Recurrent DNMT3A mutations in patients with myelodysplastic syndromes. Leukemia *25*, 1153–1158.

Wang, H., Nicolay, B.N., Chick, J.M., Gao, X., Geng, Y., Ren, H., Gao, H., Yang, G., Williams, J.A., Suski, J.M., et al. (2017). The metabolic function of cyclin D3-CDK6 kinase in cancer cell survival. Nature *546*, 426–430.

Wenger, A., Ferreyra Vega, S., Kling, T., Bontell, T.O., Jakola, A.S., and Caren, H. (2019). Intratumor DNA methylation heterogeneity in glioblastoma: implications for DNA methylation-based classification. Neuro Oncol. *21*, 616–627.

Yang, L., Rau, R., and Goodell, M.A. (2015). DNMT3A in haematological malignancies. Nat. Rev. Cancer *15*, 152–165.

Zhang, C., Zhong, J.F., Stucky, A., Chen, X.L., Press, M.F., and Zhang, X. (2015). Histone acetylation: novel target for the treatment of acute lymphoblastic leukemia. Clin. Epigenetics *7*, 117.

Zhou, W., Dinh, H.Q., Ramjan, Z., Weisenberger, D.J., Nicolet, C.M., Shen, H., Laird, P.W., and Berman, B.P. (2018). DNA methylation loss in late-replicating domains is linked to mitotic cell division. Nat. Genet. *50*, 591–602.

iScience, Volume *23*

Supplemental Information

The Effect of CDK6 Expression on DNA Methylation and DNMT3B Regulation

Gerwin Heller, Sofie Nebenfuehr, Florian Bellutti, Huriye Ünal, Markus Zojer, Lisa Scheiblecker, Veronika Sexl, and Karoline Kollmann

SUPPLEMENTAL FIGURES

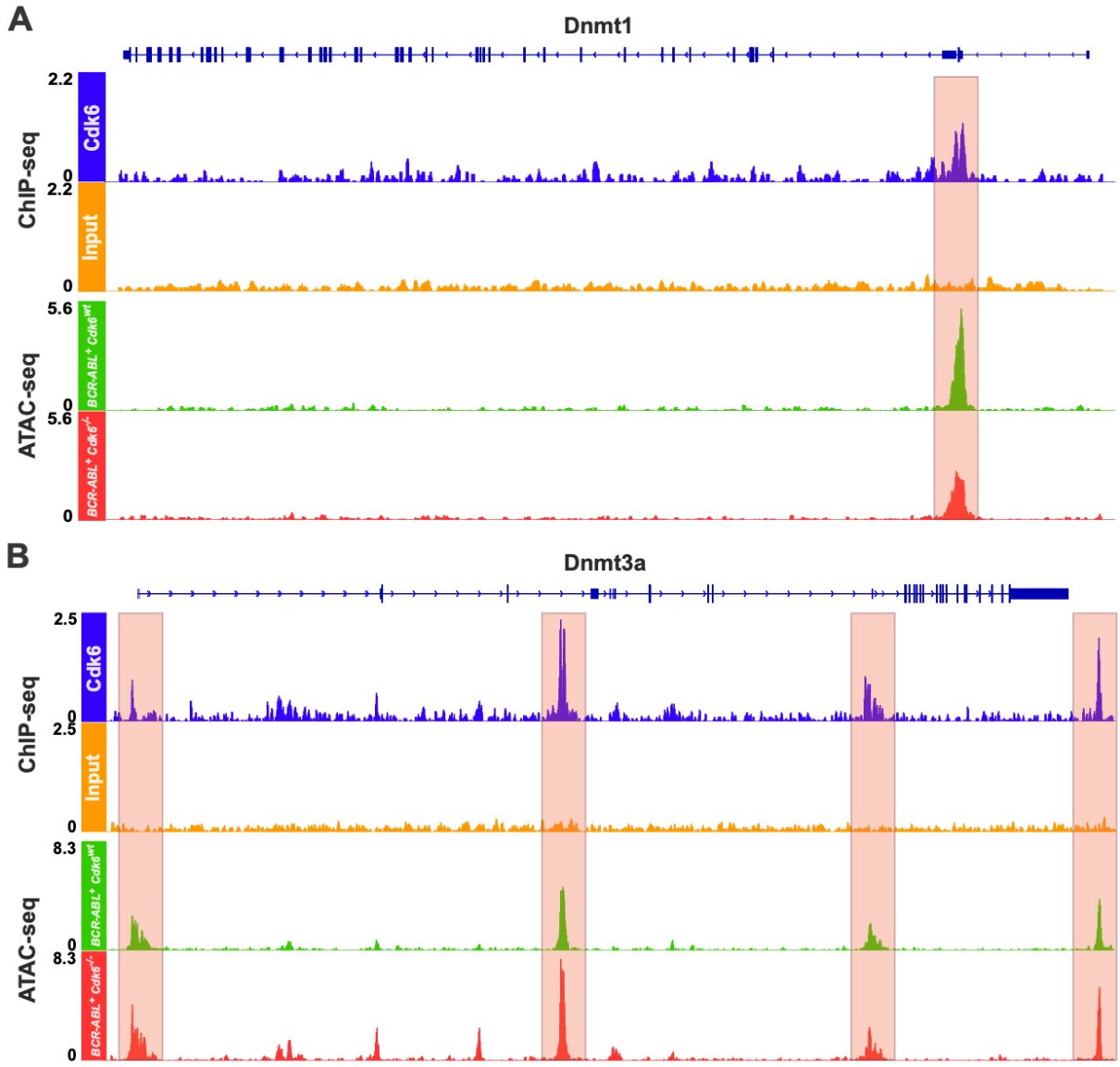

Figure S1, related to Figure 2. Binding of Cdk6 to the 5´ regions of **(A)** Dnmt1 and **(B)** Dnmt3a in *BCR-ABL*$^{+}$ cells determined by ChIP-seq analyses (upper panel). Chromatin accessibility at the 5´ regions of *Dnmt1 and Dnmt3a* in *BCR-ABL*$^{+}$ *Cdk6*^{wt} (green) and *BCR-ABL*$^{+}$ *Cdk6*$^{-/-}$ (red) cells determined by ATAC-seq analyses (lower panel).

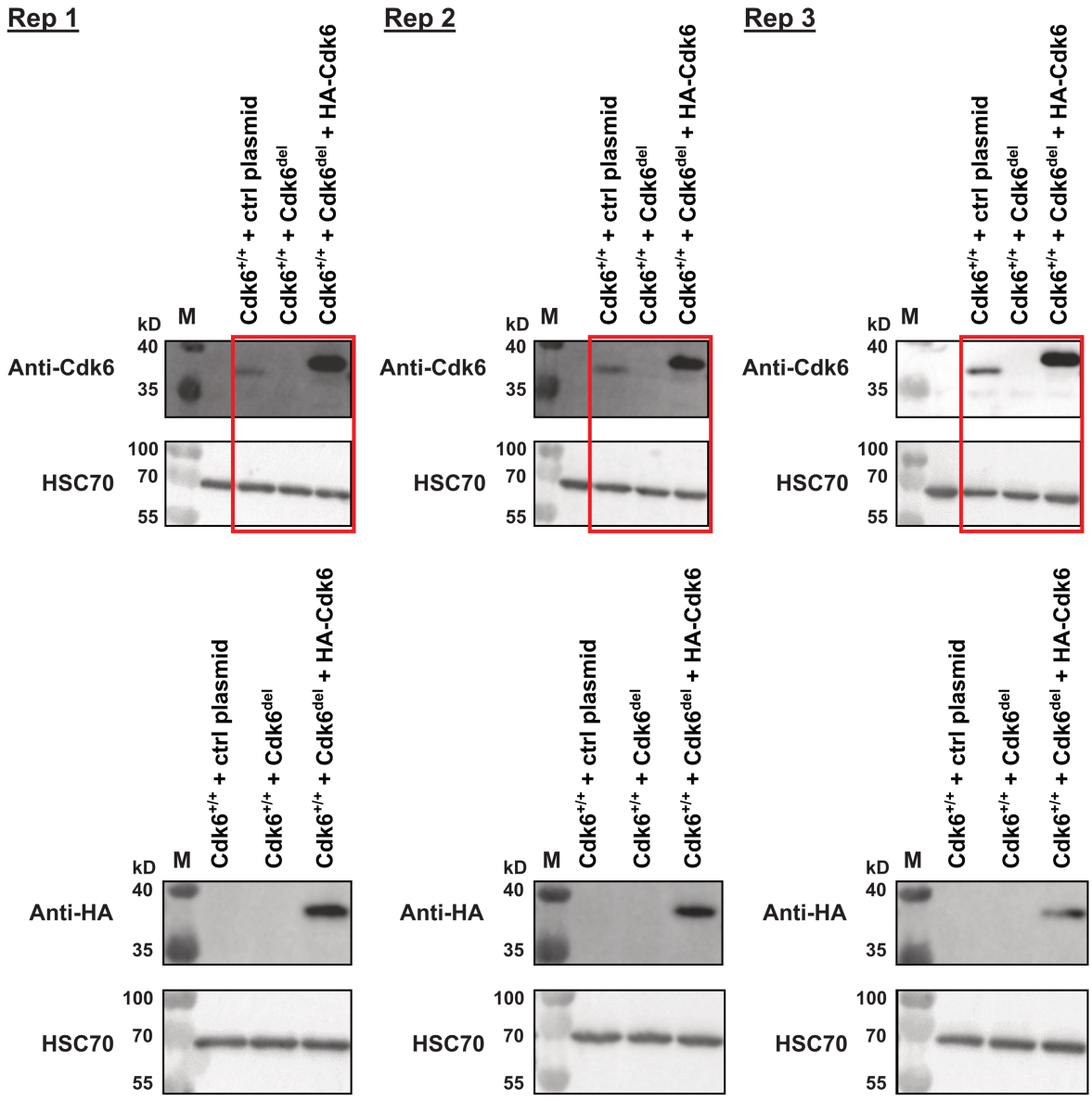

Figure S2, related to Figure 3. Western blot analyses to confirm Cdk6 loss and Cdk6 re-expression upon Cdk6 knock-out and HA-Cdk6 transduction, respectively. Results from 3 different cell lines (Rep 1-3) are shown. kD, kilodalton; M, marker.

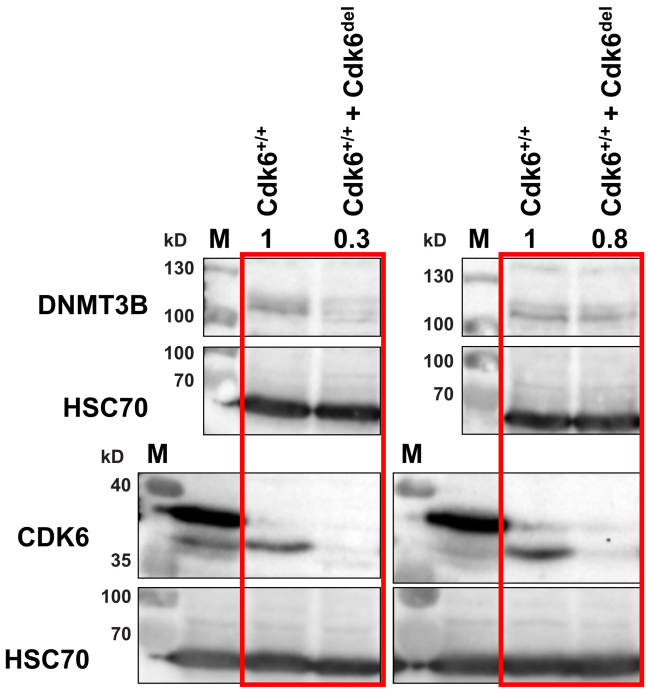

Figure S3, related to Figure 3. Western blot analyses of Dnmt3b and Cdk6 in *BCR-ABL*$^{+}$ *Cdk6*$^{+/+}$ and *BCR-ABL*$^{+}$ *Cdk6*$^{-/-}$ cell lines. Signals were densitometrically quantified and normalized to HSC70. kD, kilodalton; M, marker.

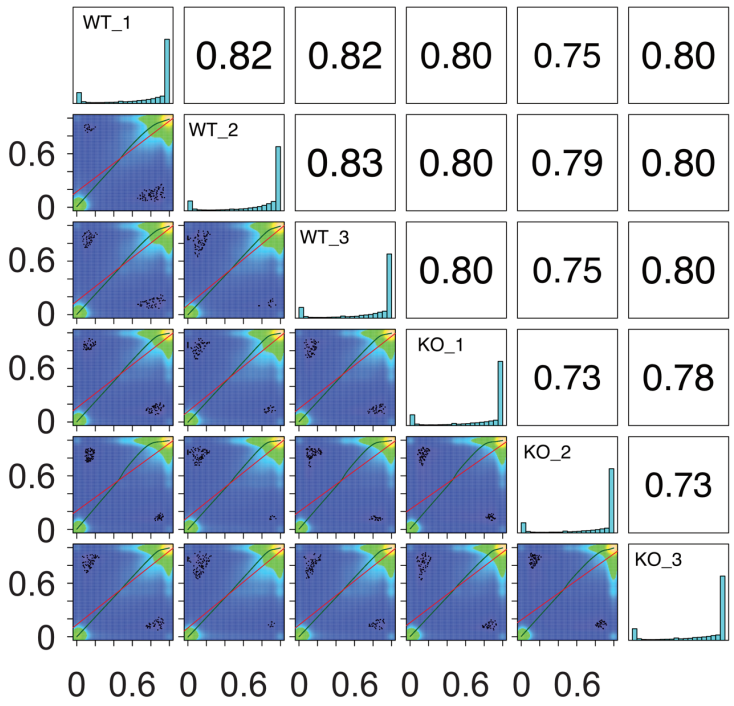

Figure S4, related to Figure 3. Correlation plot of 3 *BCR-ABL*$^{+}$ *Cdk6*^{wt} (WT) and 3 *BCR-ABL*$^{+}$ *Cdk6*$^{-/-}$ (KO) cell lines based on CpG methylation.

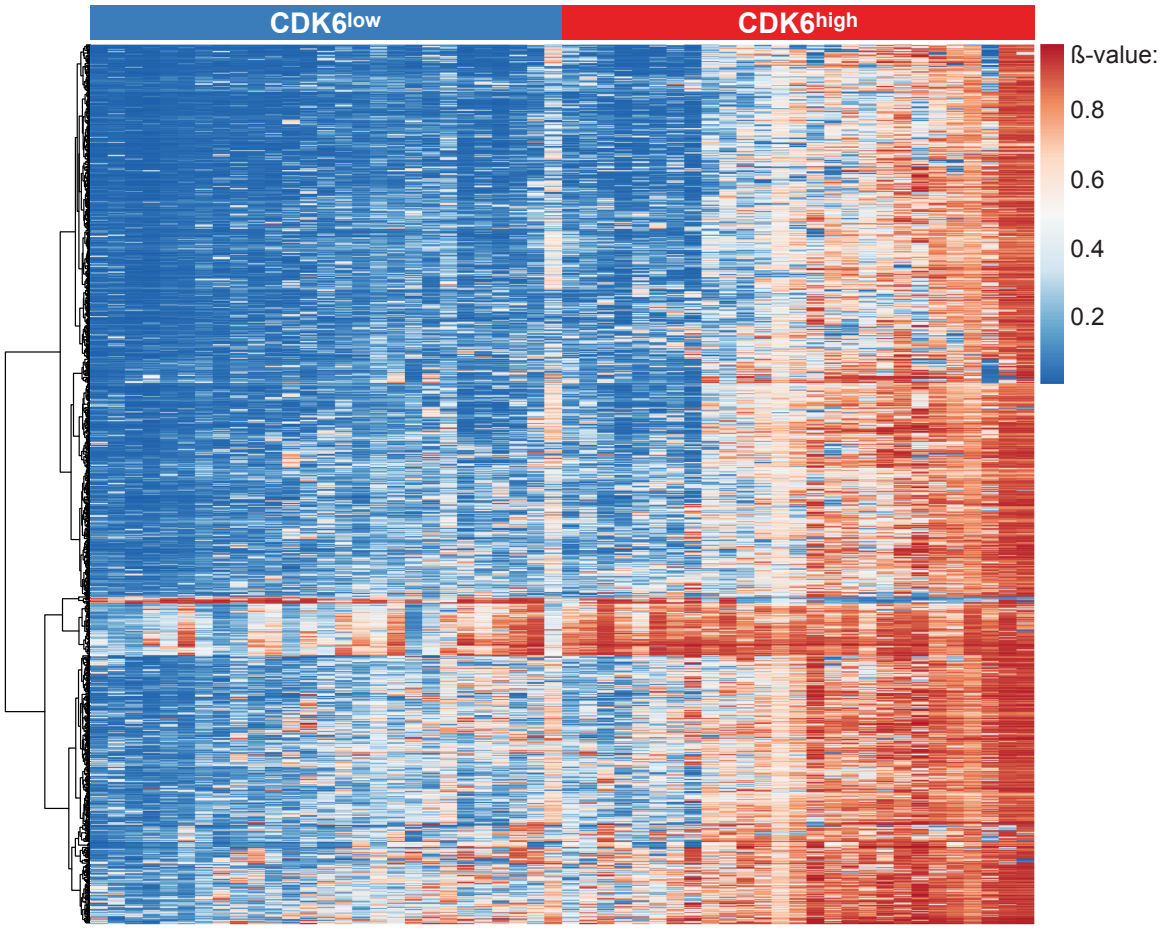

Figure S5, related to Figure 3. Heatmap showing methylation of 1,298 probes with a ß-difference of at least +/-0.3 between CDK6^{high} (upper quartile, N = 27) and CDK6^{low} (lower quartile, N = 27) AML samples from the TCGA LAML dataset. Values range from 0 (unmethylated; blue) to 1 (fully methylated; red). Each row represents a unique probe on the Infinium Human Methylation 450K BeadChip and each column represents a unique patient.

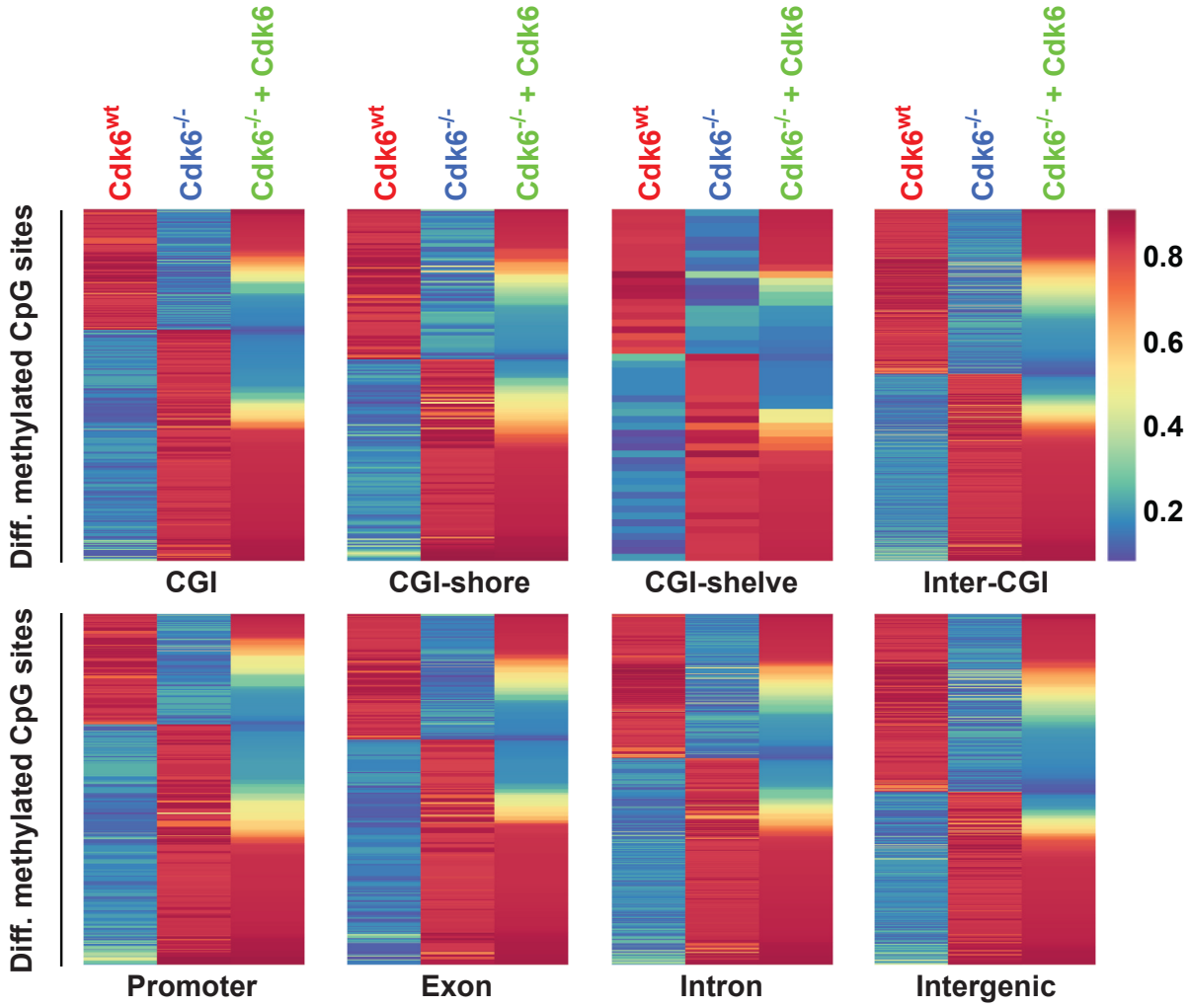

Figure S6, related to Figure 4. Heatmaps showing methylation values of differentially methylated CpG sites in 3 replicates (Rep 1-3) of *BCR-ABL*$^{+}$ *Cdk6*^{wt}, *BCR-ABL*$^{+}$ *Cdk6*$^{-/-}$ and *BCR-ABL*$^{+}$ *Cdk6*$^{-/-}$*+Cdk6* cell lines separated for CpG islands (CGI), CGI shores, CGI shelves, inter CGI regions, promoter regions, exons, introns and intergenic regions. Values are depicted as percentage of methylation and range from 0% (dark blue) to 100% (dark red).

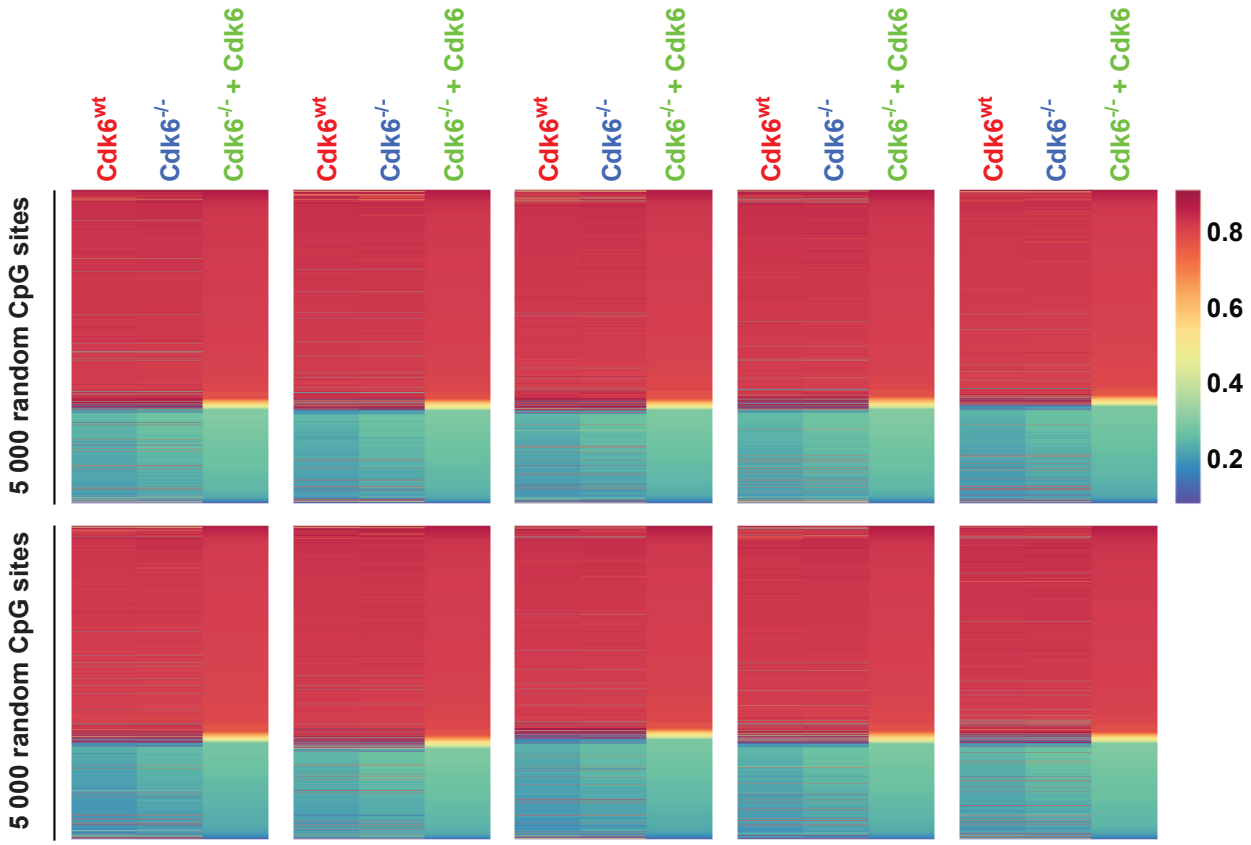

Figure S7, related to Figure 4. Heatmaps showing methylation values of 5 000 randomly selected CpG sites in *BCR-ABL*$^{+}$ *Cdk6*^{wt}, *BCR-ABL*$^{+}$ *Cdk6*$^{-/-}$ and *BCR-ABL*$^{+}$ *Cdk6*$^{-/-}$+*Cdk6* cell lines. Random CpG site selection was repeated for 10 times. Values are depicted as percentage of methylation and range from 0% (dark blue) to 100% (dark red).

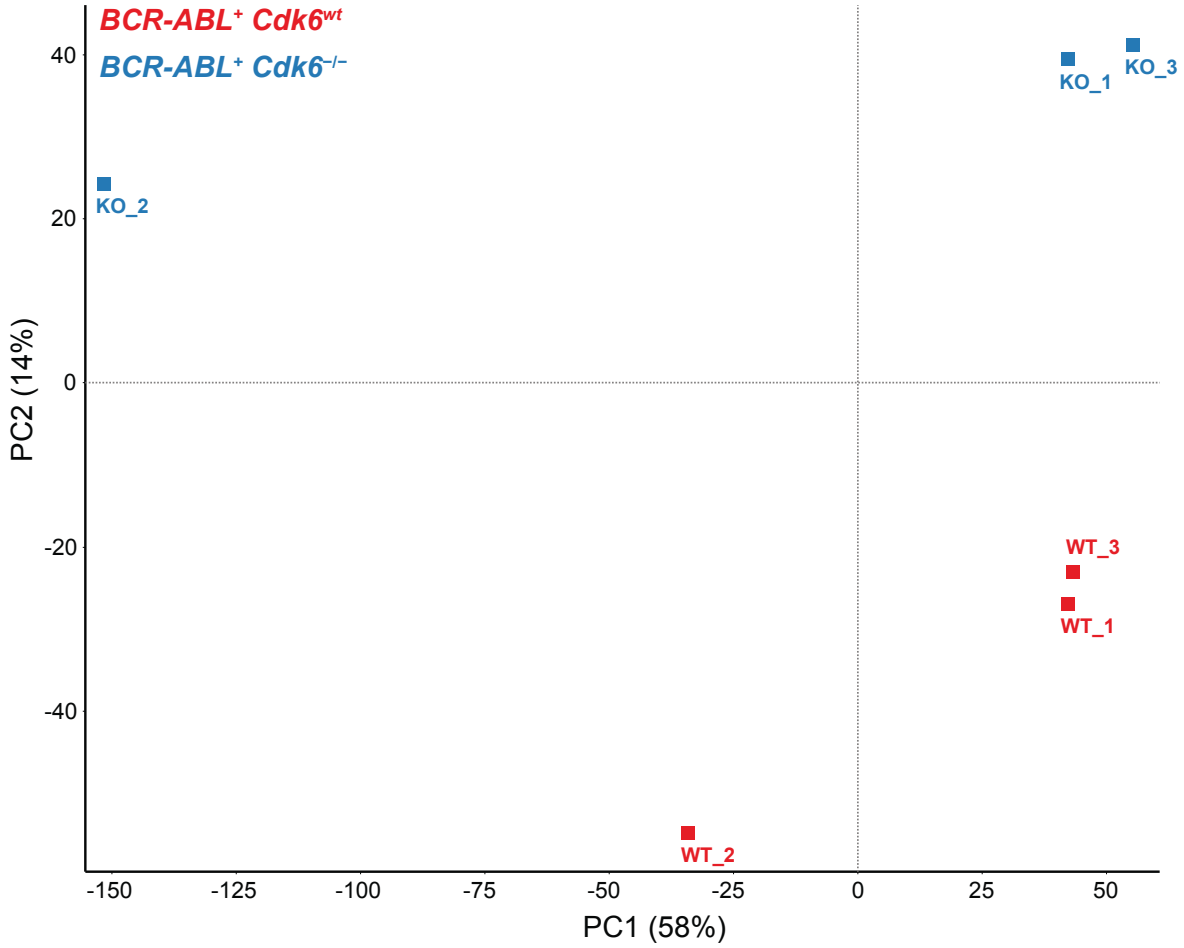

Figure S8, related to Figure 5. Principal component (PC) analysis of 3 *BCR-ABL*$^{+}$ *Cdk6*^{wt} (WT, red) and 3 *BCR-ABL*$^{+}$ *Cdk6*$^{-/-}$ (KO, blue) cell lines based on mRNA expression determined by RNA-sequencing.

TRANSPARENT METHODS

Cloning of CDK6 sgRNAs into px458 plasmid

pSpCas9(BB)-2A-GFP (px458) (plasmid number 48138; Addgene) was a gift from Krzysztof Chylinski. Cloning into px458 was performed as reported previously with slight modifications (Ran et al., 2013). The px458 plasmid was digested with BbsI (Thermofisher Scientific, Rockford, IL, USA) for 30 min at 37°C and gel purified using a Gel Extraction Kit (Qiagen, Hilden, Germany). The forward and reverse oligonucleotides (oligos) of each sgRNA were diluted at 100 µM in H_2O. The CDK6 guide oligos contain overhangs for ligation into the BbsI sites in pSpCas9(BB): forward CDK6 oligo: CACCGCCCGCGACTTGAAGAACGG, reverse CDK6 oligo: AAACCCGTTCTTCAAGTCGCGGGC. To phosphorylate and anneal the oligos, 2 µg of each oligo were mixed with T4 ligation buffer and T4 PNK (New England Biolabs, NEB, Ipswich, MA, USA) to a final volume of 20 µl and incubated for 1h at 37°C (phosphorylation), followed by 5 min at 95°C and then ramping down the temperature to 20°C at -1°C/min (annealing). Annealed and phosphorylated oligos were diluted 1:10 in H_2O. Ligation reactions for each sgRNA were performed by mixing 10 ng of the digested and purified px458 plasmid with 90 ng of the diluted phosphorylated and annealed oligos, T4 ligation buffer, and T4 ligase (NEB) in a final volume of 10 µl. Ligation was carried out for 16 h at 16°C. Chemically competent DHL5 bacteria were transformed and plated on LB plates containing 50 mg/ml ampicillin. Plates were incubated overnight at 37°C. Colonies were checked for correct insertion of the sgRNA by PCR colony screening, followed by sequencing (U6 primer: GAGGGCCTATTTCCCATGATTCC).

Gene editing in BCR-ABL+ cell lines

BCR-ABL+ cell lines were maintained in RPMI medium supplemented with 10% FCS, 50 µmol/L 2-mercaptoethanol, 100 U/mL penicillin, and 100 µg/mL streptomycin (PAA, Linz, Austria). Cells were electroporated (one single pulse with a voltage of 1600 V and a pulse width of 20 ms; NeonTM Transfection System, Invitrogen, Carlsbad, CA, USA) with 1µg control plasmid pSpCas9(BB)-2A-GFP(px458) or the plasmid expressing sgRNAs against CDK6 pSpCas9(BB)-2A-GFP(px458)-hCDK6del. For each transfection, $2x10^5$ cells were resuspended in Buffer R (Neon™) in a reaction volume of 10µl. Transfected cells were cultured in RPMI (supplemented with 10% FCS and 50 µmol/L 2-mercaptoethanol) for 24h. GFP^+ cells were sorted using a FACSAria™ II cell sorter (BD Biosciences, San Jose, CA, USA) and plated as single cell suspension into 96-well plates. For the re-expression of HA-CDK6, pMSCV-IRES-GFP plasmids were used. The outgrowth of clones was monitored by microscopic inspection. Cells are routinely tested for mycoplasma contamination.

RNA extraction and Real-Time PCR

Total RNA was extracted from cell lines using the RNeasy Mini Kit (Qiagen) as recommended by the manufacturer. Reverse transcription was performed using the iSCRIPT cDNA synthesis kit (Bio-Rad). All qPCRs were performed in duplicate with the SsoFastTM EvaGreen®Supermix (Bio-Rad) according to the instructions of the manufacturer. Primer sequences for Dnmt3b were as follows: fwd, 5´-GTGGTGCACTGAGCTCGAAAGGATCTTCG-3´ and rev, 5´-ATCACAGGCAAAGTAGTCCTTCAAGG-3´ (Kweon et al., 2017). Levels of mRNAs were normalized to Rplp0 mRNA.

Western Blotting

Protein lysates were prepared using RIPA lysis buffer supplemented with cOmplete™ Protease Inhibitor tablet (Roche Diagnostics, Indianapolis, IN, USA), separated by SDS/PAGE and transferred onto nitrocellulose blotting membrane (Amersham™ Protran™ 0.45µm NC, GE Healthcare, Life Sciences). Membranes were blocked in 5% BSA followed by incubation with primary antibodies: anti-CDK6 (1:1000, H-96, Santa Cruz, Dallas, TX, USA), anti-HA (1:1000, ab9110, Abcam, Cambridge, UK), anti-Dnmt3b (1:1000, ab122932, Abcam) and anti-HSC70 (1:1000, B-6, Santa Cruz). Appropriate secondary HRP antibodies (1:10000, Cell Signaling Technology, Danvers, MA, USA) were used and membranes were visualized using Clarity™ ECL Western blotting substrate (Biorad, Hercules, CA, USA).

Reduced Representation Bisulfite Sequencing (RRBS)

RRBS was performed as reported previously (Heller et al., 2016). In brief, genomic DNA was MspI (NEB) digested, end-repaired and A-tailed using Klenow Polymerase (NEB) followed by adapter ligation using Quick Ligase (NEB) and AMPure XP size selection (Beckman Coulter, Fullerton, CA, USA). RRBS libraries were sodium bisulfite treated using the EZ-DNA Methylation-Direct kit (Zymo Research Corp, Orange, CA, USA) and quantified by qPCR. Enrichment PCR was performed using the PfuTurboCx Hotstart Kit (Agilent Technologies, Santa Clara, CA, USA) followed by AMPure XP clean up. Quality of final RRBS libraries was determined by Experion analysis (Biorad). Sequencing was performed on a HiSeq2000 sequencer (Illumina Inc, San Diego, CA, USA). RRBS reads were processed using the --

rrbs option of the *Trim Galore!* software and *bismark* was used to align reads to GRCm38 and for methylation calling (Krueger and Andrews, 2011). Differential methylation analysis and data visualization were performed using the R packages *DSS* (v2.32.0), *methylKit* (v1.10.0), *EnhancedVolcano* (v1.2.0) and *ggplot2* (v3.2.1). RRBS data are deposited in the Gene Expression Omnibus (GEO) database (Accession ID: GSE145220).

RNA-seq

Total RNA was prepared using the RNeasy Kit (Qiagen) and processed for sequencing using the TruSeq RNA Sample Preparation Kit (Illumina Inc, San Diego, CA, USA). RNA-seq reads were processed using *Trim Galore!* software (http://www.bioinformatics.babraham.ac.uk/projects/trim_galore/) and aligned to GRCm38 using *STAR* (Dobin et al., 2013). Data visualization was done using ClustVis (Metsalu and Vilo, 2015). Gene Ontology analysis were performed using Ontologizer (Bauer et al., 2008) and visualized using the R package GOplot (Walter et al., 2015). RNA-seq data are deposited in the Gene Expression Omnibus (GEO) database (Accession ID: GSE156966, GSE145220).

ChIP-seq

CDK6 chromatin immunoprecipitation (ChIP) was performed using an antibody against HA (ab9110, Abcam) as described previously (Bellutti et al., 2018, Scheicher et al., 2015). Cells were crosslinked with DSG (20 minutes, RT) and 1% formaldehyde (10 minutes, RT) and termination of the fixation procedure was performed using glycine. For immunoprecipitation (IP), 70 µl Dynabeads Protein G magnetic beads (Invitrogen) were used, IP DNA was subjected to sequencing library preparation and sequencing was performed using the Illumina HiSeq3000/4000 platform. Raw sequencing reads were quality controlled using FASTQC followed by quality filtering, trimming of reads and adapter removal using trimmomatic (v0.36). Mapping against the mouse reference genome (Gencode M13) was done using bwa-mem (v0.7.15) and blacklisted regions were removed using bedtools subtract (v2.26.0). Multimappers and reads with bad mapping quality were removed using samtools (v1.3.1). Peak calling was performed by MACS2 (v2.1.0) using default parameters and motif identification was performed using Homer (v4.9.0) findMotifsGenome.pl with the default -size 200. ChIP-seq data are deposited in the Gene Expression Omnibus (GEO) database (Accession ID: GSE113752).

ATAC-seq

10^5 cells were washed once in 50 µl PBS and resuspended in transposase reaction mix (12.5 µl 2 × TD buffer, 2 µl transposase (Illumina), 10.5 µl nuclease-free water and 0.01% NP-40). Tagmentation was performed for 30 min at 37 °C. The optimum number of amplification cycles was estimated by qPCR reaction as previously described (Rendeiro et al., 2016). Following library amplification, fragments larger than 1 200 bp were excluded by SPRI size selection. DNA concentration was measured using a Qubit fluorometer (Invitrogen). Libraries were amplified using custom Nextera primers (Buenrostro et al., 2013) and sequenced by the Biomedical Sequencing Facility at CeMM using the Illumina HiSeq3000/4000 platform. ATAC-seq data are deposited in the Gene Expression Omnibus (GEO) database (Accession ID: GSE156966).

Chromatome analysis

Chromatome analyses were performed as described previously (Dutta et al., 2012, Bellutti et al., 2018). Briefly, the purified chromatin pellet was subjected to Benzonase digestion and solubilized in SDS lysis buffer. Filter Aided Sample Prep (FASP) was performed according to the procedure described previously (Wisniewski et al., 2009). Peptides were desalted using C18 solid phase extraction spin columns (The Nest Group, Southborough, MA) labeled with TMT 6plex™ reagents (Pierce, Rockford, IL) and pooled. Organic solvent was removed in vacuum concentrator and labelled peptides were loaded onto a solid phase extraction column. Peptides were eluted with 300µL 80% acetonitrile containing 0.1% trifluoroacetic to achieve a final peptide concentration of ~1µg/µl. Eluate was then used for phosphopeptide enrichment applying a modified method of immobilized metal affinity chromatography (IMAC) (Ficarro et al., 2005). Briefly, two times 100 µL of Ni-NTA superflow slurry (Qiagen) were washed with LCMS-grade water and Ni^{2+} stripped off the beads by incubation with 100 mM of EDTA, pH 8 solution for 1 h at room temperature. Stripped NTA resin was recharged with Fe^{3+}-ions by incubation with a fresh solution of $Fe(III)Cl_3$ and 75 µL of charged resin used for the enrichment of a total of ~300 µg TMT-labelled peptide. The unbound fraction was transferred to a fresh glass vial and used for offline fractionation for the analysis of the whole chromatome proteome. After washing the slurry with 0.1% TFA, phosphopeptides were eluted with a freshly prepared ammonia solution containing 3mM EDTA, pH 8 and all used for offline fractionation for the analysis of the phosphoproteome. Offline fractionation via RP-HPLC at pH 10 and 2D-RP/RP Liquid Chromatography Mass Spectrometry were performed as described (Bellutti et al., 2018). Raw data files were processed using the Proteome Discoverer 2.2.0. platform, utilizing the Sequest HT database search engine and Percolator validation software node

(V3.04) to remove false positives with a false discovery rate (FDR) of 1% on peptide and protein level under strict conditions. Searches were performed with full tryptic digestion against the mouse SwissProt database v2017.12 (25 293 sequences and appended known contaminants) with up to two miscleavage sites (Bellutti et al., 2018). For statistical analysis and p-value calculation, the integrated ANOVA hypothesis test was used. TMT ratios with p-values below 0.01 were considered statistically significant.

Publicly available datasets and co-expression analysis

The following human ALL Affymetrix HG-U133_plus_2.0 gene expression microarray datasets were obtained from ArrayExpress database: E-MTAB-5035, E-GEOD-13351, E-GEOD-49032 and E-GEOD-13576. Spearman correlation coefficients of log2 expression values were calculated using the “cor” function of R and data visualization was done using the “corrplot” package. ETS1 ChIP-seq data were obtained from GEO database: GSM803442, GSM803468, GSE83758. Infinium Human Methylation 450K BeadChip data of AML patients were obtained from the Cancer Genome Atlas database (LAML dataset).

SUPPLEMENTAL REFERENCES

BAUER, S., GROSSMANN, S., VINGRON, M. & ROBINSON, P. N. 2008. Ontologizer 2.0--a multifunctional tool for GO term enrichment analysis and data exploration. *Bioinformatics,* 24**,** 1650-1.

BELLUTTI, F., TIGAN, A. S., NEBENFUEHR, S., DOLEZAL, M., ZOJER, M., GRAUSENBURGER, R., HARTENBERGER, S., KOLLMANN, S., DOMA, E., PRCHAL-MURPHY, M., URAS, I. Z., HOLLEIN, A., NEUBERG, D. S., EBERT, B. L., RINGLER, A., MUELLER, A. C., LOIZOU, J. I., HINDS, P. W., VOGL, C., HELLER, G., KUBICEK, S., ZUBER, J., MALUMBRES, M., FARLIK, M., VILLUNGER, A., KOLLMANN, K. & SEXL, V. 2018. CDK6 Antagonizes p53-Induced Responses during Tumorigenesis. *Cancer Discov,* 8**,** 884-897.

BUENROSTRO, J. D., GIRESI, P. G., ZABA, L. C., CHANG, H. Y. & GREENLEAF, W. J. 2013. Transposition of native chromatin for fast and sensitive epigenomic profiling of open chromatin, DNA-binding proteins and nucleosome position. *Nat Methods,* 10**,** 1213-8.

DOBIN, A., DAVIS, C. A., SCHLESINGER, F., DRENKOW, J., ZALESKI, C., JHA, S., BATUT, P., CHAISSON, M. & GINGERAS, T. R. 2013. STAR: ultrafast universal RNA-seq aligner. *Bioinformatics,* 29**,** 15-21.

DUTTA, B., ADAV, S. S., KOH, C. G., LIM, S. K., MESHORER, E. & SZE, S. K. 2012. Elucidating the temporal dynamics of chromatin-associated protein release upon DNA digestion by quantitative proteomic approach. *J Proteomics,* 75**,** 5493-506.

FICARRO, S. B., SALOMON, A. R., BRILL, L. M., MASON, D. E., STETTLER-GILL, M., BROCK, A. & PETERS, E. C. 2005. Automated immobilized metal affinity chromatography/nano-liquid chromatography/electrospray ionization mass spectrometry platform for profiling protein phosphorylation sites. *Rapid Commun Mass Spectrom,* 19**,** 57-71.

HELLER, G., TOPAKIAN, T., ALTENBERGER, C., CERNY-REITERER, S., HERNDLHOFER, S., ZIEGLER, B., DATLINGER, P., BYRGAZOV, K., BOCK, C., MANNHALTER, C., HORMANN, G., SPERR, W. R., LION, T., ZIELINSKI, C. C., VALENT, P. & ZOCHBAUER-MULLER, S. 2016. Next-generation sequencing identifies major DNA methylation changes during progression of Ph+ chronic myeloid leukemia. *Leukemia,* 30**,** 1861-8.

KRUEGER, F. & ANDREWS, S. R. 2011. Bismark: a flexible aligner and methylation caller for Bisulfite-Seq applications. *Bioinformatics,* 27**,** 1571-2.

KWEON, S. M., ZHU, B., CHEN, Y., ARAVIND, L., XU, S. Y. & FELDMAN, D. E. 2017. Erasure of Tet-Oxidized 5-Methylcytosine by a SRAP Nuclease. *Cell Rep,* 21**,** 482-494.

METSALU, T. & VILO, J. 2015. ClustVis: a web tool for visualizing clustering of multivariate data using Principal Component Analysis and heatmap. *Nucleic Acids Res,* 43**,** W566-70.

RAN, F. A., HSU, P. D., WRIGHT, J., AGARWALA, V., SCOTT, D. A. & ZHANG, F. 2013. Genome engineering using the CRISPR-Cas9 system. *Nat Protoc,* 8**,** 2281-2308.

RENDEIRO, A. F., SCHMIDL, C., STREFFORD, J. C., WALEWSKA, R., DAVIS, Z., FARLIK, M., OSCIER, D. & BOCK, C. 2016. Chromatin accessibility maps of chronic lymphocytic leukaemia identify subtype-specific epigenome signatures and transcription regulatory networks. *Nat Commun,* 7**,** 11938.

SCHEICHER, R., HOELBL-KOVACIC, A., BELLUTTI, F., TIGAN, A. S., PRCHAL-MURPHY, M., HELLER, G., SCHNECKENLEITHNER, C., SALAZAR-ROA, M., ZOCHBAUER-MULLER, S., ZUBER, J., MALUMBRES, M., KOLLMANN, K. & SEXL, V. 2015. CDK6 as a key regulator of hematopoietic and leukemic stem cell activation. *Blood,* 125**,** 90-101.

WALTER, W., SANCHEZ-CABO, F. & RICOTE, M. 2015. GOplot: an R package for visually combining expression data with functional analysis. *Bioinformatics,* 31**,** 2912-4.

WISNIEWSKI, J. R., ZOUGMAN, A., NAGARAJ, N. & MANN, M. 2009. Universal sample preparation method for proteome analysis. *Nat Methods,* 6**,** 359-62.